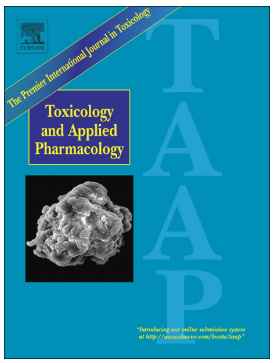

A novel bile acid analog, A17, ameliorated non-alcoholic steatohepatitis in high-fat diet-fed hamsters

Ying Wang, Yao Zhu, Junxing Niu, Qiangqiang Deng, Shimeng Guo, Haowen Jiang, Zhaoliang Peng, Yaru Xue, Huige Peng, Lijiang Xuan, Guoyu Pan

PII: S0041-008X(20)30295-7

DOI: https://doi.org/10.1016/j.taap.2020.115169

Reference: YTAAP 115169

To appear in: *Toxicology and Applied Pharmacology*

Received date: 9 May 2020

Revised date: 12 July 2020

Accepted date: 27 July 2020

Please cite this article as: Y. Wang, Y. Zhu, J. Niu, et al., A novel bile acid analog, A17, ameliorated non-alcoholic steatohepatitis in high-fat diet-fed hamsters, *Toxicology and Applied Pharmacology* (2020), https://doi.org/10.1016/j.taap.2020.115169

A novel bile acid analog, A17, ameliorated non-alcoholic steatohepatitis in high-fat diet-fed hamsters

Ying Wang[ab#], Yao Zhu[ab#], Junxing Niu[ab], Qiangqiang Deng[ab], Shimeng Guo[abc], Haowen Jiang[abc], Zhaoliang Peng[ab], Yaru Xue[ab], Huige Peng[ab], Lijiang Xuan[ab*], Guoyu Pan[ab*]

[a]*Shanghai Institute of Materia Medica, Chinese Academy of Sciences, Shanghai 201203, China*

[b]*University of Chinese Academy of Sciences, Beijing 100049, China*

[c]*National Center for Drug Screening, Shanghai 201203, China*

[#]These authors contributed equally to this work.

*Corresponding authors.

Guoyu Pan, Ph.D., Professor

Shanghai Institute of Materia Medica

Chinese Academy of Sciences

501 Hai-ke Rd, Shanghai, 201203

Tel: +86-21-20231000 ext 1715

Email: gypan@simm.ac.cn

Lijiang Xuan, Ph.D., Professor,

Shanghai Institute of Materia Medica

Chinese Academy of Sciences

501 Hai-ke Rd, Shanghai, 201203

Tel: +86-21-20231968

Email: ljxuan@simm.ac.cn

Abstract

Being endocrine signaling molecules that regulate lipid metabolism and affect energy balance, bile acids are potential drug candidates for non-alcoholic steatohepatitis (NASH). Obeticholic acid (OCA) could improve NASH accompanied by significant side effects. Therefore, it is worthwhile to develop safer and more effective bile acid analogs. In this study, a new bile acid analog A17 was synthesized and its potential anti-NASH effects were assessed *in vitro* and *in vivo*. The impact of A17 on steatosis was investigated in the rat primary hepatocytes challenged with oleic acid. It was found that A17 alleviated lipid accumulation by reducing fatty acid (FA) uptake and promoting FA oxidation. The reduction of FA uptake came from inhibiting fatty acid translocase (Cd36) expression. The promoting of FA oxidation came from stimulating the phosphorylation of adenosine monophosphate (AMP)-activated protein kinase alpha (AMPKα). In addition, A17 reduced lipopolysaccharide-induced inflammation in Raw264.7 cells by activating Takeda G protein-coupled receptor 5 (TGR5). In *in vivo* study, male Golden Syrian hamsters were fed with high fat (HF) diet and then treated with 50 mg/kg A17 for 6 weeks. A17 lowered the lipid profile and liver enzyme levels in serum and improved liver pathological conditions with less side effects compared with OCA. Further studies confirmed that the molecular mechanisms of A17 *in vivo* were similar to those *in vitro*. In conclusion, a novel bile acid analog A17 was identified to ameliorate NASH in HF-fed hamsters. The potential mechanisms could be contributed to reducing FA uptake, stimulating FA oxidation and relieving inflammation.

Keywords: bile acid analog; NASH; TGR5; Cd36; AMPKα.

Introduction

Non-alcoholic fatty liver disease (NAFLD) has become the most common chronic liver disease around the world [1], which comprises non-alcoholic fatty liver (NAFL) and non-alcoholic steatohepatitis (NASH) [2]. NAFL is the first stage of NAFLD and considered as a benign condition [3], which is featured by simple lipid accumulation (i.e. lipid accumulation in ≥ 5% hepatocytes) in clinic [4]. Though NAFL can be reversed via changing lifestyle and treating with lipid-lowering medicine [5], 10-25% patients progress to NASH [6], which is regarded as a more serious disease with intralobular inflammation, hepatocyte ballooning and damage [7]. Moreover, compared to NAFL patients, the patients with NASH carry a higher risk of adverse hepatic outcomes including fibrosis, cirrhosis and hepatocellular carcinoma (HCC) [8]. Increasing data demonstrates that the recent elevation in HCC incidence is driven by NASH in developed countries [9]. Hence, NASH is of the major health concern worldwide.

The pathogenesis of NASH is complex and multifactorial [10]. So far, the most popular theory is 'two hits hypothesis'. The first hit is intrahepatic lipid accumulation, which results from four mechanisms, namely (1) the increase in hepatic fatty acids (FA) uptake, (2) the increase in liver lipolysis, (3) the reduction of mitochondrial FA oxidation and (4) the reduction of triglycerides (TG) export from the liver [11]. These lipid metabolism abnormalities sensitize the liver to a 'second hit', such as the induction of oxidation stress and the excess production of inflammatory cytokines, resulting in the progression to NASH [12].

Bile acids (BAs) are endocrine signaling molecules that regulate lipid and glucose metabolism and affect energy balance [13]. The function of BAs in regulating lipid metabolism is mediated by activating the nuclear farnesoid X receptor (FXR) [14]. FXR activation reduces hepatic lipogenesis and promotes FA oxidation, which results in the decreases of hepatic lipid

accumulation [15]. Another main receptor of BAs is Takeda G protein-coupled receptor 5 (TGR5) whose activation increases energy expenditure, improves glucose tolerance and inhibits inflammation [16]. Interestingly, total BAs concentrations and the primary to secondary BAs ratio are increased in NASH patients [17]. Moreover, the increase in circulating BAs level is relevant to the metabolic benefits after bariatric surgery [18]. These appearances indicate that BAs may take an important part in the development, progression, and regression of NASH.

Considering the effects of BAs signaling on lipid homeostasis and energy expenditure, modulating BAs receptor activities is a promising therapeutic strategy to treat NASH. Obeticholic acid (OCA), a chenodeoxycholic acid derivative, is a potent and selective FXR agonist [19]. Clinical results indicated that OCA improved the liver histologic score in NASH patients and may become the first approved agent to treat NASH. However, OCA resulted in a concentration-dependent pruritus and elevated total cholesterol (TC) and LDL-cholesterol (LDL-C) levels in serum, which increased cardiovascular risk [20]. INT-777, a cholic acid derivative, is a potent and selective TGR5 agonist [21]. Administration of INT-777 in high fat (HF) diet-fed C57BL/6J mice ameliorated hepatic steatosis and decreased liver enzyme levels [22]. In addition, dual agonist of FXR and TGR5, INT-767, which is also a bile acid analog, reduced hepatic lipid accumulation and proinflammatory cytokine expression in *db/db* obese mice [23]. Notably, norursodesoxycholic acid, a side-chain shortened derivative of ursodesoxycholic acid (UDCA), was found to ameliorate NASH in mouse models [24] and clinic [25] without activating FXR or TGR5, suggesting that bile acid analogs may have the potential to treat NASH with different mechanisms.

Given that preclinical and clinical studies of bile acid analogs in treating NASH are promising, other bile acid analogs deserve intensively explored to develop safer and more effective therapies, which may have different pharmacological mechanisms from exist. In this report, a new bile acid analog A17 was synthesized by protecting the sensitive hydroxyl groups and using condensation agent to connect amino acids. A17 was found to reduced lipid accumulation in oleic acid (OA)-induced rat primary hepatocytes (RPHs) steatosis model and inhibit lipopolysaccharide (LPS)-induced inflammation in Raw264.7. It also ameliorated NASH in HF-induced hamsters by reducing lipid uptake, promoting FA oxidation and inhibiting inflammation in liver. The reduction of lipid uptake came from inhibiting the expression of fatty acid translocase (Cd36). The promoting of FA oxidation came from stimulating adenosine monophosphate (AMP)-activated protein kinase alpha (AMPKα)/acetyl-CoA carboxylase (ACC)/carnitine palmitoyltransferase-1α (Cpt-1α) pathway. The anti-inflammation effect came from activating TGR5/nuclear factor of kappa light polypeptide gene enhancer in B-cells inhibitor alpha (IκBα) pathway.

Materials and Methods

The synthetic routes of A17

UDCA (1.0 mmol) was dissolved in anhydrous tetrahydrofuran (THF, 10 mL), under N_2 protection, 5 mL 98% HCOOH and 20 μL 70% $HClO_4$ were added at the same time under stirring at 55°C. And then, the mixture was stirred at 55°C for 2-4 h and subjected to evaporation of the solvent to generate compound 1. Under N_2 protection, compound 1 (1.0 mmol), HATU (1.2 mmol) and L-(+)-VALINOL (1.3 mmol) was dissolved in anhydrous

dichloromethane (DCM, 15 mL). Under stirring, triethylamine (TEA, 170 μL, 1.5 mmol) was added to the mixture, which was then stirred at room temperature for 3-4 h, generating the target compound A17. Silica gel column chromatography (petroleum ether: acetone = 8:1 ~ 3:1, v:v, contains 0.1% formic acid); Yield 82%; White Powder; ^{1}H NMR (400 MHz, $CDCl_3$) δ 8.05 (s, 1H), 8.01 (s, 1H), 4.80 – 4.70 (m, 2H), 3.66 (td, J = 6.5, 4.6 Hz, 1H), 3.53 (qd, J = 11.2, 5.4 Hz, 2H), 3.29 (q, J = 1.7 Hz, 1H), 2.28 (dd, J = 8.9, 4.6 Hz, 1H), 2.18 – 2.08 (m, 1H), 2.04 (dd, J = 12.5, 3.4 Hz, 1H), 1.91 – 1.80 (m, 4H), 1.79 – 1.69 (m, 4H), 1.68 – 1.55 (m, 4H), 1.54 – 1.36 (m, 6H), 1.36 – 1.28 (m, 3H), 1.24 – 1.15 (m, 1H), 1.15 – 1.03 (m, 2H), 1.00 (s, 3H), 0.96(d, J = 6.3 Hz, 3H), 0.92 (d, J = 6.8 Hz, 3H), 0.83 (d, J = 6.8 Hz, 3H), 0.70 (s, 3H). ESI-MS: m/z 534.4 $[M + H]^+$; HRMS (ESI): m/z calcd. For $C_{31}H_{52}NO_6^+$ $[M + H]^+$534.3795, found 534.3767.

Fatty acid preparation

50 mM sodium oleate (Sigma-Aldrich, Saint Louis, MO, USA) stock was prepared in 50% ethyl alcohol by heating at 70°C for 2 min. Meanwhile, 2% fatty acids-free bovine serum albumin (BSA, Sigma-Aldrich, Saint Louis, MO, USA) was dissolved in William's E medium (GIBCO, GrandIsland, NY, USA) and preheated at 37°C. After completely vortexed, the sodium oleate stock was added into 2% BSA dropwise to make 2.5 mM OA-BSA conjugate and mixed completely at 37°C on a shaker for 1 h. The conjugate was later filtered with 0.25 μM pore sized polyvinylidene fluoride hydrophilic membrane filter and stored at -20°C.

Hepatocytes culture and steatosis induction

Isolated RPHs were suspended in plating medium and plated onto collagen-coated 96-well (3×10^4 cells/well) plate. After 4 h incubation in a humidified atmosphere containing 95% air and 5% CO_2 at 37°C, RPHs adhered to the collagen completely and spread out. Then, the medium was replaced with feeding medium containing 100, 250, 500, 750, 1000 μM OA. Corresponding concentrations of BSA were used as negative controls. Post 24 h treatment, cells were assayed for their viability and intracellular TG levels.

Hepatocytes intracellular A17 measurement

RPHs were seeded in collagen-coated 6-well (1×10^6 cells/well) plates and treated with 10, 25 or 50 μM A17 for 24 h. After washed with phosphate buffer solution (PBS) for 3 times, the cells were collected and intracellular A17 concentrations were detected using HPLC/MS-8030 triple quadrupole system (Shimadzu Corp, Kyoto, Japan). The positive electrospray ionization interface (ESI) mode was chosen. A17 and the internal standard (tolbutamide) were separated by Sunfire C18 columns (2.1 ×100 mm, i.d. 3.5 μm). The precursor and product ion values were *m/z* 534.2 (Q1) > *m/z* 442.3 (Q3) for A17 and *m/z* 271.0 (Q1) > *m/z* 172.0 (Q3) for tolbutamide, with collision energy (CE) of 23 eV and 20 eV respectively. The mobile phase (MP) consisted of acetonitrile (A) and 0.1% formic acid (C) with a gradient elution of 60% MPC at 0-0.1 min, 5% MPC at 1-2 min, and 60% MPC at 3-7 min, at a flow rate of 0.25 mL/min. The oven temperature was 40 °C, and the injection volume was 20 μL.

Hepatocytes chemical treatment

As shown in the results section, 500 μM OA was chosen to induce RPHs steatosis model. RPHs were seeded in collagen-coated 96-well (3×10^4 cells/well) and 6-well (1×10^6 cells/well) plates. After attached to the collagen, the cells were treated with 500 μM OA and 10 μM or 25 μM A17 for 24 h. OCA (purity > 98%, Dalian Meilun Biotechnology Co., LTD, Dalian, China) at the same concentrations were used as positive controls and 0.1% dimethyl sulfoxide (DMSO, Sigma-Aldrich, Saint Louis, MO, USA) was used as a negative control. Cells in the 96-well plate was assayed for viability, intracellular TG levels and fatty acid uptake, while those in the 6-well plate were harvested for intracellular malondialdehyde (MDA) concentration measurement, qPCR and western blot assay.

In another experiment, RPHs were seeded in collagen-coated 96-well (3×10^4 cells/well) and pretreated with or without 10 μM Etomoxir (Selleck Chemicals, Houston, TX, USA), which is a Cpt-1α irreversible inhibitor, for 24 h. Then, RPHs were treated with or without 500 μM OA, 25 μM A17 and 10 μM Etomoxir for another 24 h. Intracellular TG levels and cell viability were measured.

FXR binding assay

The binding potency of A17 to FXR was determined by AlphaScreen-GST detection kit (PerkinElmer, Waltham, MA, USA) according to the manufacturer's instructions. OCA was used as positive control. After different concentrations of A17 reacted with GST-FXR system for 2 h at room temperature, the ligand-induced interaction between the steroid receptor coactivator 1 (SRC1) and FXR were detected by an EnVision multiplate reader (PerkinElmer, Waltham, MA, USA).

HEK293 transient transfection and TGR5 activation assay

Human embryonic kidney (HEK) 293 cell line was purchased from the American Type Culture Collection (ATCC, Manassas, VA, USA) and maintained in Dulbecco's modified Eagle's medium (DMEM) containing 10% fetal bovine serum (FBS, GIBCO, GrandIsland, NY, USA) and 1% streptomycin/penicillin (GIBCO, GrandIsland, NY, USA). Human TGR5 plasmid was obtained from the UMR cDNA Resource Center (Rolla, MO, USA). Nearly 2 × 10^6 HEK293 cells were suspended in 200 μL transfection buffer and were transiently transfected with human TGR5 plasmid by electroporation, which was performed with a Scientz-2C electroporation apparatus (Scientz Biotech, Ningbo, China). Intracellular cyclic-AMP (cAMP) of TGR5-transfected HEK293 treated with different concentrations of A17 was measured as described previously [26]. INT-777 (MedChemExpress, Monmouth Junction, NJ, USA) at the same concentrations were used as positive controls and 0.1% DMSO was used as a negative control.

Raw264.7 culture and treatment

Mouse macrophage cell line Raw264.7 was obtained from ATCC and maintained in DMEM-High Glucose medium containing 10% FBS. When the confluent reached 90%, the cells were seeded on 6-well (6 × 10^5 cells/well) plate. After 12 h culture, the cells were pretreated with 25 μM A17 for 24 h. 10 μM dexamethasone (Dex, Sigma-Aldrich, Saint Louis, MO, USA) was used as a positive control and 0.1% DMSO was used as a negative control. Subsequently, the cells were simulated with 1 μg/mL LPS (Sigma-Aldrich, Saint Louis, MO,

USA) supplemented with 25 μM A17 or 10 μM Dex for another 8 h. the supernatants were collected for nitric oxide (NO), tumor necrosis factor alpha (TNF-α) and interleukin-6 (IL-6) measurement.

In another experiment, the cells were seeded on 6-well and pretreated with 25 μM A17 for 24 h. 25 μM INT-777 was used as a positive control and 0.1% DMSO was used as a negative control. Afterwards, the cells were simulated with 1 μg/mL LPS supplemented with 25 μM A17 or 25 μM INT-777 for another 1 h, and then harvested for western blot assay.

Cell viability assay

Cell viability was evaluated by Cell Counting Kit 8 (CCK8, Yeasen Biotech Co. Ltd, Shanghai, China) according to the manufacturer's instructions. Briefly, after the cells in 96-well plates underwent different treatments for 24 h, 10 μL CCK8 was added to each well and incubated for another 1 h. The absorbance of 450 nm was measured by the automatic microplate reader (Biotek, Winooski, VT, USA).

Cellular TG measurements

The content of TG in cells was measured to determine the extent of steatosis. At the end of the treatment, the cells in 96-well plates were washed with PBS and lysed by 10% Triton (Beyotime Biotechnology, Shanghai, China) for 30 min. the lysates of each well were collected and measured by commercial kits (Nanjing Jiancheng Bioengineering Institute, Nanjing, China) following the protocol of manufacturer. The absorbance at 510 nm was assayed and the results were normalized to protein concentration measured by Pierce BCA

Protein Assay Kit (Thermo Fisher Scientific, Madison, WI, USA).

Cellular malondialdehyde (MDA) measurements

Intracellular MDA concentration was measured to examine the effect of A17 on lipid peroxidation. After treatment of OA and A17 or OCA, the cells in 6-well plates were washed with PBS and lysed by RIPA buffer (Beyotime Biotechnology, Shanghai, China), the lysates of each well were collected and measured by commercial kits (Beyotime Biotechnology, Shanghai, China) following the instructions of manufacturer. The absorbance at 532 nm was assayed and the results were normalized to protein concentration.

Fatty acid uptake assay

Free fatty acid uptake assays (Molecular Devices, San Jose, USA) were performed after the cells in 96-well plates were incubated with compounds for 24 h. 10 μM Triacsin C (Sigma-Aldrich, Saint Louis, MO, USA) served as positive control and incubated with cells for 2 h before the assay. Assay buffer containing BODIPY®-dodecanoic acid fluorescent fatty acid analog (BODIPY® 500/512 C1, C12[1]) coupled with quench was prepared and added 100 μL to each well. Then, the excitation/emission 485/515 nm was read immediately using a kinetic mode (every 1 min for 30 min). For blank wells, the compound diluent was added, and the fluorescence was subtracted from the values for those wells with cells treated with compounds. The results were normalized to cell viability measured by CCK-8.

Fatty acid oxidation (FAO) assay

The oxygen consumption rate (OCR) due to oxidation of fatty acids was measured using a Seahorse XFe96 extracellular flux analyzer (Agilent Technologies, Santa Clara, California). RPHs were seeded into collagen coated 96-well Seahorse microplates at 1×10^4 cells/well. Four hours later, media was replaced with feeding medium containing 500 μM OA and 25 μM A17 or OCA, 50 μM amiodarone was used as positive control. After 24 h treatment, OCR was measured as previously described in the protocol [27]. The median antimycin/rotenone (A/R) measurements at time point 10, 11 and 12 was subtracted from the median of FCCP measurements at time point 7, 8 and 9 to identify chemical effects on maximal respiration.

Measurement of NO and inflammatory cytokines

NO assay was conducted using commercial kit (Beyotime Biotechnology, Shanghai, China). TNF-α and IL-6 levels were quantified with mouse TNF-α and IL-6 ELISA kits (Multi Sciences Biotech. Co. Ltd, Hangzhou, China). All the operations were strictly performed according to the operating manual.

Animal experiments

The animal experiments were performed according to protocols approved by the Institutional Animal Care and Use Committee (IACUC) of Shanghai Institute of Materia Medica, People's Republic of China Academic Science. Male Sprague-Dawley rats (180 ± 10 g, IACUC permission number: 2018-05-PGY-24) and Male Golden Syrian hamsters (100 ± 10 g, IACUC permission number: 2019-05-PGY-32) were purchased from Shanghai SLAC Laboratory Animal Co. (Shanghai, People's Republic of China) and housed under controlled

temperature (23 ± 2°C), relative humidity (50 ± 10%) and lighting (12 h light/dark cycle). Experiments were performed after animals were acclimated for 7 days.

RPHs were isolated from male Sprague-Dawley rats by two-step collagenase perfusion following the previous protocols [28].

Hamsters were fed a standard diet (n = 10) or a HF diet (n = 15) containing 60% fat (#12492, Research Diets, Inc., New Brunswick, NJ, USA), and provided with normal drinking water. The weights of animals were measured once a week until the end of the experiment.

After 16 weeks of diet, the hamsters fed the standard diet were randomly divided into two groups (n = 5 per group) and were given a daily dose of A17 at 50 mg/kg (A17 group) or vehicle (vehicle group) by intraperitoneal injection. Hamsters under HF diet were kept on the same diet and allocated into the following 3 treatment groups (n = 5 per group): (1) HF group, the HF diet group treated with vehicle daily by intraperitoneal injection; (2) HF + OCA group, the HF diet group treated with OCA at 20 mg/kg/d by oral gavage and (3) HF + A17 group, the HF diet group treated with A17 at 50 mg/kg/d by intraperitoneal injection. The drug treatment lasted for 6 weeks. OCA was suspended in 0.5% carboxyl-methyl cellulose (Sigma-Aldrich, Saint Louis, MO, USA) and sonicated for 1 h to form homogenous liquid. A17 was distributed in 20% hydroxypropyl-beta-cyclodextrin (purity > 98%, Dalian Meilun Biotechnology Co., LTD, Dalian, China) and sonicated overnight to get clear liquid.

At the end of the study, serum samples were collected after an overnight fast for determination of serum TG, TC, LDL-C, alanine aminotransferase (ALT) and aspartate aminotransferase (AST) levels. Then, hamsters were euthanized and livers were immediately

removed, washed and cut into two parts. One part of the livers was fixed in 4% formaldehyde solution to perform histology analysis, the other was stored at -80℃ for lipid measurement, qPCR and western blot assay.

Biochemical analysis

The serum TG, TC, LDL-C, ALT and AST concentrations were assayed using commercial kits (Nanjing Jiancheng Bioengineering Institute, Nanjing, China) according to the manufacturer's protocols.

For the measurements of the TG and TC levels in liver, liver samples were homogenized in 9-fold diluted absolute ethyl alcohol and centrifuged at 2500 rpm for 10 min at 4°C. The supernatants were collected for analysis using commercial available kits (Nanjing Jiancheng Bioengineering Institute, Nanjing, China).

Histology analysis and scoring

The liver tissue samples fixed in 4% formaldehyde solution were embedded in paraffin and subsequently stained with Hematoxylin-Eosin (H & E) and Oil Red. After staining, steatosis and inflammation variables of each liver slices were assessed based on a previous reported scoring system [29] in a blinded way by Zuocheng Biotechnology Co., LTD, Shanghai, China.

RNA extraction and real-time PCR analysis

Total RNA was extracted from cells and liver samples by TRIzol reagent (Life

Technology, CA, USA) and purified with the EZ-10 Spin column & Collection Tube (Sangon Biotech, Shanghai, China). Then, isolated RNA was dissolved in water-DEPC treated water (Sangon Biotech, Shanghai, China) and quantitated using the ScanDrop 100 spectrophotometer (Analytik Jena, Jena, German). 1000 ng of total RNA was reversely transcribed into cDNA using PrimeScript™ RT Master Mix (Takara, Shiga, Japan) by T100™ thermal cycler (Bio-Rad, Hercules, California). Later, 2 μL cDNA was used as template in a 20 μL PCR mix containing 7.2 μL water-DEPC treated water, 0.4 μL each forward and reverse primers (Sangon Biotech, Shanghai, China) and 10 μL Hieff® qPCR SYBR Green Master Mix (Low Rox Plus, Yeasen Biotech, Shanghai, China) for PCR setup. PCR reactions were performed using the Applied Biosystems™ 7500 Fast real-time PCR system (Thermo Fisher Scientific, Madison, WI, USA) following the manufacture's protocol. Primers for genes were list in Table 1. The detective mRNA levels were normalized against Gapdh.

Western blot analysis

Total protein was extracted with RIPA buffer supplemented with 1% protease inhibitor cocktail (Sigma-Aldrich, Saint Louis, MO, USA) and quantitated using Pierce BCA Protein Assay Kit (Thermo Fisher Scientific, Madison, WI, USA). After diluted to the same concentration and conjugated to the sodium dodecyl sulfate (SDS) by being heated at 95°C for 10 min, the proteins were separated on a 10% denaturing SDS gel and then transferred to polyvinylindene difluoride membrane (Merck Millipore, Darmstadt, Germany). Then, the blots were blocked using 5% skim milk in TBS-T (25 mM Tris-HCl pH 7.6, 150 mM NaCl, 2.5 mM KCl and 0.3% Tween-20) for 1 h at room temperature and incubated with the

following primary antibodies overnight at 4°C. Gapdh (1:2000), p-AMPKα (1:1000), AMPKα (1:1000), p-ACC (1:1000), ACC (1:1000), p-IκBα (1:1000) and IκBα (1:1000) were bought from Cell Signaling Technology (Danvers, MA, USA); β-actin (1:1000),Cpt-1α (1:1000), fatty acid binding protein (plasma membrane) (Fabp[pm], 1:1000), fatty acid transport protein 2 (Fatp2, 1:1000) and IL-6 (1:1000) were purchased from Proteintech Group (Wuhan, China); fatty acid transport protein 5 (Fatp5, 1:1000) and Cd36 (1:1000) were from Abcam (Cambridge, MA, USA). After washing with TBS-T, the blots were incubated with respective secondary antibodies (1:10000, Yeasen Biotech, Shanghai, China) at room temperature for 1 h. Later, the protein bands were soaked with the electrochemiluminescence (ECL) detection reagent (Thermo Fisher Scientific, Madison, WI, USA) and captured by the ChemiScope 3300 mini system (CLINX, Shanghai, China). The relative blot intensity of each group was quantified by Image J software (National Institute of Health, MD, USA).

Statistical analysis

All the data were analyzed using GraphPad Prism 7.0 software (GraphPad Software Inc., La Jolla, CA) and represent as mean ± SD. The Student's t test was used to precede the comparison between two groups. One-way analysis of variance (ANOVA) was used in case of multiple testing. *$P < 0.05$, **$P < 0.01$, ***$P < 0.001$ were shown as statistical difference, and the significance increases progressively.

Results

Synthesis of A17

Previous researches showed that modifications of carboxyl in the C17 side chain could improve the activities of BAs in activating FXR/TGR5 [30-32]. In contrast, bile acid synthetic intermediates which lack carboxyl or hydroxyl in the C17 side chain showed no effects on FXR/TGR5 activation [33]. These evidences suggest that the C17 side chain of BAs has a large pocket with hydrogen bond donor/acceptor groups [34]. Considering the reactivity of carboxyl groups, amide was formed to connect different hydrogen bond donors and receptor groups. In addition, to prevent the hydroxyl reaction, formyl was used to protect and replace the hydroxyl to form new hydrogen bond receptor groups. Thus, A17 was synthesized by connecting amino acids to the C17 side chain of UDCA and protecting the sensitive hydroxyl groups using formyl.

The synthesis of A17 started from commercially available UDCA; formylation of UDCA in HCOOH gave compound 1, which then reacted with L-(+)-VALINOL to form A17 in the presence of HATU and TEA (Scheme 1).

A17 ameliorated OA-induced steatosis in rat primary hepatocytes

Given that A17 could be transported into RPHs (Fig. S1), RPHs induced by OA was chosen to be the cell model to assess the effect of A17 on steatosis *in vitro*. OA (≥ 500 μM) caused a significant decrease in cell viability and increase in TG accumulation (Fig. 1A-B). Therefore, 500 μM OA was used to induce lipid accumulation in RPHs in the later experiments. OCA could decrease intracellular TG concentrations dose-dependently in OA-induced RPHs (Fig. S2), so it was used as the positive control. A17 treatment dramatically reduced intracellular TG level and increased viability in a dose-dependent

manner in RPHs induced by OA (Fig. 1C-D). In addition, excessive lipid peroxidation results in oxidation stress, which is a hallmark of NASH progression [35]. Thus, Intracellular MDA concentrations were measured and found to be lowered to normal value in OA-induced RPHs after A17 treatment ($p < .05$, Fig. 1E). Notably. The inhibitory effect of A17 on steatosis was greater than that of OCA. These results indicated that A17 alleviated steatosis in OA-induced RPHs model.

A17 treatment inhibited FA uptake via reducing Cd36 protein expression

Lipid accumulation in hepatocytes partly attributes to the increase in lipid influx. Hence, the effect of A17 on hepatocellular FA uptake was measured. Triacsin C, a long-chain acyl-CoA synthetases inhibitor was used as positive control. 25 μM A17 significantly inhibited the uptake of FA in RPHs induced by OA ($p < .001$), while 25 μM OCA made no differences (Fig. 2A). Western blot analysis demonstrated that A17 treatment significantly decreased the expression of Cd36 ($p < .01$), but not other FA uptake transporters like Fabp(pm) , Fatp2 and Fatp5 (Fig. 2B). These results suggested that A17 decreased the protein level of Cd36, which resulted in the reduction of FA entered into hepatocytes.

A17 treatment promoted FA oxidation via AMPKα/ACC/Cpt-1α pathway

Hepatocellular lipid accumulation also depends on energy balance, especially fatty acid oxidation. In hepatocytes, fatty acid are broken down in mitochondria to provide energy by beta-oxidative pathways which require oxygen consumption [36]. Thus, the OCR was measured to assess FA oxidation. RPHs induced by OA showed significant lower OCR

compared to the vehicle group ($p < .001$, Fig. 3A), which could be one of the causes of lipid accumulation. 25 μM A17 markedly increased FA oxidation in RPHs induced by OA ($p < .001$), while 25 μM OCA made no differences in OCR (Fig. 3A). Analysis of the proteins involved in fatty acid oxidation revealed that 25 μM A17 increased the expression of Cpt-1α ($p < .01$) and the phosphorylation levels of AMPKα and ACC ($p < .05$, $p < .05$, Fig. 3B). Additionally, the mRNA expression of Cpt-1α was significantly elevated by A17 treatment ($p < .001$, Fig. 3C). Further inhibitor experiment showed that Cpt-1α inhibitor Etomoxir (10 μM) significantly reversed the effects of A17 on reducing intracellular TG levels ($p < .05$, Fig. 3D) and increasing cell viability ($p < .001$, Fig. 3E). These results suggested that A17 increased the expression of Cpt-1α by AMPKα/ACC pathway, promoting FA oxidation and clearing intracellular fatty acids.

A17 activated TGR5 and inhibited inflammatory response in Raw264.7

Being a bile acid analog, A17 may be the ligand of FXR and/or TGR5. To verify if the potential anti-steatosis function of A17 was relevant to FXR activation, the binding potency of A17 to FXR was measured. Compared to OCA whose EC_{50} was 201.55 nM, A17 was unable to bind FXR (Fig. 4A) and thus could not activate FXR directly. Furthermore, the mRNA levels of FXR-targeted genes such as small heterodimer partner (Shp), bile salt export pump (Bsep) and cytochrome P450 7a1 (Cyp7a1) were not affected by A17 in OA-induced RPHs (Fig. S3A) or *in vivo* (Fig. S3B), implying that A17 was not an agonist of FXR.

The effect of A17 on TGR5 was further investigated. A17 was an activator of TGR5 with an EC_{50} of 117.5 nM, reaching 90% response of INT-777 (Fig. 4B). Activating TGR5 in

macrophages has been reported to suppress multiple inflammatory diseases by blunting the phosphorylation of IκBα [37]. To further verify the effect of A17 on TGR5 activation, the potential anti-inflammation function of A17 in LPS-induced Raw264.7 cell model was evaluated. Pretreating with 25 μM A17 for 24 h significantly inhibited NO, TNF-α and IL-6 levels in the supernatant of LPS-induced Raw264.7 ($p < .001$, $p < .01$, $p < .05$, Fig. 4C). A17 also decreased phosphorylation of IκBα ($p < .05$, Fig. 4D), implying A17 attenuated LPS-induced cytokine expression via TGR5/IκBα pathway.

A17 administration ameliorated steatosis and inhibited inflammatory response in hamsters

After feeding HF diets for 16 weeks, the body weights of the hamsters in HF group were markedly increased compared to that of control group ($p < .001$, Fig. 5A). Administration of A17 for 6 weeks slightly decreased the weights of hamsters compared to HF group, while no weight loss were found in HF + OCA group (Fig. 5A).

The serum biochemistry results (Table 2) revealed that HF diets dramatically increased the levels of lipid parameters such as TG, TC, LDL-C, ALT and AST ($p < .001$, $p < .01$, $p < .01$, $p < .001$, $p < .001$). Compared to those in HF group, hamsters in HF + A17 group showed a down-regulated profile in serum lipid parameters, with lower TG by 50% ($p < .001$), decreased TC and LDL-C levels by 26% and 32% ($p < .05$, $p < .05$), respectively. It is worthwhile to note that OCA treatment did not change serum TC and LDL-C levels. Besides, hamsters in HF + A17 group had significant lower serum ALT and AST levels by 75% and 85% ($p < .001$, $p < .001$), respectively, which were even lower than those of HF + OCA group.

Consistent with the results of serum biochemistry, liver Oil Red and H & E staining indicated that hamsters in HF group showed severe fatty accumulation and inflammation with the score of 5.4 and 4.8 ($p < .001$, $p < .001$), respectively. Administration of A17 resulted in reversal of hepatic steatosis and inflammation and lowered the score to 2.8 and 1.8 ($p < .001$, $p < .001$, Fig. 5B-C), respectively. Measurement of the TG levels in liver further confirmed that A17 significantly alleviated steatosis compared to the HF-fed hamsters ($p < .001$). However, the TC level in liver was neither reduced by OCA nor A17 (Table 2). Altogether, these findings indicated that A17 prevented liver injury in HF-induced NASH model.

A17 alleviated NASH via inhibiting Cd36, stimulating AMPKα/ACC/Cpt-1α pathway and TGR5/IκBα pathway

Western blot results showed that HF induced a significant increase in the protein level of Cd36 ($p < .01$), which was dramatically reversed by A17 treatment ($p < .001$), but neither HF nor A17 changed the expression of other FA uptake transporters such as Fabp(pm), Fatp2 or Fatp5 (Fig. 6A). In regard to FA oxidation, HF inhibited the AMPK signaling pathway by markedly decreasing the ratios of p-AMPKα/AMPKα and p-ACC/ACC ($p < .001$, $p < .001$), while A17 treatment elevated the phosphorylation of AMPKα and ACC ($p < .05$, $p < .05$), which resulted in the increase of Cpt-1α expression ($p < .01$, Fig. 6B). Moreover, A17 significantly increased the mRNA expression of Cpt-1α in hamster livers (Fig. 6C). These results showed that the anti-steatosis mechanism of A17 in hamsters was in accordance to that in RPHs. In addition, A17 treatment substantially decreased the production of p-IκBα and IL-6 ($p < .001$, $p < .001$) in liver induced by HF ($p < .001$, $p < .001$, Fig. 6D), suggesting that

A17 suppressed cytokine production by activating the TGR5 in liver.

Discussion

Although NASH is a complex and multisystem disease, one of its most important end points is lipid accumulation [38]. Therefore, OA-induced RPH steatosis model was applied to assess the anti-steatosis effect of A17 *in vitro*. It was found that A17: (1) dramatically reduced intracellular TG and MDA levels and increased hepatocyte viability (Fig. 1); (2) inhibited FA uptake via reducing Cd36 protein expression (Fig. 2); and (3) promoted FA oxidation via AMPKα/ACC/Cpt-1α pathway (Fig. 3). Then, A17 was found to be an agonist of TGR5 and inhibited LPS-induced inflammation in Raw264.7 via TGR5/IκBα pathway (Fig. 4). Further animal studies confirmed that A17 alleviated NASH in HF-induced hamsters (Fig. 5), and the mechanism was the same as that *in vitro* (Fig. 6).

In this report, A17 was found to be a potent TGR5 agonist (Fig. 4B). Previous studies have reported that the specific TGR agonist INT-777 inhibited LPS-induced inflammation in Raw264.7 model [39] and hepatic inflammatory response in mice via antagonizing NF-κB [40]. Consistent with these results, A17 treatment in Raw264.7 significantly reduced the phosphorylation of IκBα and resulted in decreased NO, IL-6 and TNF-α concentrations in supernatant, confirming that the anti-inflammatory effect of A17 was link with TGR5 activation (Fig. 4C-D). In the liver, TGR5 is expressed in Kupffer cells, which are the resident macrophages [37]. The TGR5 expressed in Kupffer cells may enable A17 to attenuate hepatic inflammation in hamsters developed NASH. Decreasing the lipid content in liver and reducing inflammation have been two therapeutic directions to treat NASH. Notably, besides

diminishing inflammation, A17 ameliorated steatosis in both OA-induced RPHs and hamster model of NASH by inhibiting FA uptake and stimulating FA oxidation in hepatocytes, implying parenchymal hepatic cells was another action site of A17. In contrast, INT-777 had no effects on steatosis in OA-induced RPHs (Fig. S4). Though INT-777 was reported to reduce hepatic steatosis and obesity in high-fat feeding C57BL/6J mice, the underlying mechanism was the activation of TGR5 in brown adipose/muscle tissue and intestinal L cells [22]. Therefore, not only the activation of TGR5 in Kupffer cells, but also the direct action on hepatocytes contributed to the anti-NASH effect of A17.

Compared to OCA, which directly acts on hepatocytes by activating FXR, A17 had no agonistic effect on FXR (Fig. 4A), suggesting their mechanisms are quite different. FXR activation reduces hepatic lipogenesis via inhibiting the expression of hepatic sterol responsive element binding protein 1c [41] and promotes FA oxidation by inducing peroxisome proliferator-activated receptor alpha [42]. However, our results indicated the elevation effect of OCA on FA oxidation was not as great as that of A17 in OA-induced RPHs (Fig. 3A). Moreover, OCA had no effects on FA uptake, which was markedly inhibited by A17 (Fig. 2A). Regarding safety issues, increased TC and LDL-C levels in NASH patients, which increases the risk of cardiovascular diseases, is a significant side effect of OCA in clinical trials. In contrast, hamster experiment results indicated that A17 markedly decreased the serum TC and LDL-C contents (Table 2), implying the lower risk of developing related adverse event. Furthermore, treating HF-fed hamsters with 30 mg/kg/d OCA for 2 weeks dramatically lowered the weight of animals and increased ALT, AST and bilirubin (TBIL) levels in serum ($p < .01$, $p < .01$, $p < .001$, Fig. S5). While administrating HF-fed hamsters with 50 mg/kg/d

A17 for 6 weeks did not show any liver injuries (Fig. 5B-C). Therefore the safety window of A17 was much wider than that of OCA.

Hepatic FA uptake is mainly mediated by the scavenger receptor Cd36 and the Fatp family (Fatp2 and Fatp5) [43]. The expression of Cd36 is low in hepatocytes under normal conditions, but could be drastically enhanced in livers of obese and diabetic murine models [44]. Moreover, in human NAFLD, Cd36 expression correlates with liver TG content and insulin resistance [45], implying that Cd36 is important in regulating hepatic lipid content under high FA flux conditions. Disruption of hepatic Cd36 in HF-fed mice protected them against inflammation and insulin resistance [46], which highlights the possibility of treating NAFLD via modulating FA uptake in liver. A17 was found to decrease the protein expression of Cd36 (Fig. 2B), which resulted in the reduction of FA uptake. However, the mechanism remains to be determined. Cd36 was reported to be a shared target of liver X receptor, pregnane X receptor and peroxisome proliferator-activated receptor gamma, and the former two regulation were liver-specific [47]. Therefore, the regulation of Cd36 may be mediated by nuclear receptors. In addition, it was reported that specific bile acids can inhibit the function of hepatic fatty acid uptake transporters. For example, UDCA and deoxycholic acid are the potent inhibitors of Fatp5 [48]. As a bile acid analog, A17 has the potential to be the inhibitor of hepatic fatty acid uptake transporters as well. Considering the high expression of Cd36 on macrophages, adipocytes, cardiomyocytes and muscle cells [49], the potential side effect of A17 will be addressed in a future study.

AMPK serves as an energy sensor in cellular metabolism, harmonizing metabolic pathways and maintaining the energy balance [50]. Liver-specific activation of AMPK has been

reported to prevent mice from high-fructose-induced steatosis [51]. In this report, A17 upregulated the phosphorylation level of AMPKα, and phosphate-AMPKα past phosphorylation to ACC. Phosphate-ACC decreased the level of malonyl-CoA, which has inhibitory effect on Cpt-1α. Thereby, phosphorylating AMPKα indirectly activated Cpt-1α to promote fatty acid β-oxidation. Previous studied have proved that Cd36 overexpression elevated the src kinase Fyn mediated liver kinase B1 phosphorylation, which hindered the activation of AMPK [52]. While inhibiting the palmitoylation of Cd36 enhanced the phosphorylation of AMPK, promoting FA oxidation and inhibiting lipid accumulation [53]. Whether the stimulation effect of A17 on AMPKα phosphorylation is relevant to Cd36 deserves further research.

In summary, our study suggested A17, a novel bile acid analog, ameliorated NASH in HF-fed hamsters in three ways, reducing FA uptake via inhibiting the expression of Cd36, stimulating FA oxidation via AMPKα/ACC/Cpt-1α pathway, and relieving inflammation via TGR5/IκBα pathway (Fig. 7).

Author contributions

Ying Wang, Guoyu Pan, Junxing Niu and Lijiang Xuan designed the research; Ying Wang, Yao Zhu, Qiangqiang Deng, Shimeng Guo, Haowen Jiang, Zhaoliang Peng, Yaru Xue conducted the experiments; Ying Wang, Shimeng Guo, Haowen Jiang and Zhaoliang Peng were responsible for the data analysis; Ying Wang and Guoyu Pan wrote the manuscript; Yao Zhu, Shimeng Guo, Huige Peng and Lijiang Xuan helped revise the manuscript. All the authors reviewed and agreed on the final version.

Declaration of competing interest

The authors declare no competing financial interests.

Acknowledgements

This study was supported by the 'Organ Reconstruction and Manufacturing' Strategic Priority Research Program of the Chinese Academy of Sciences [grant number XDA16020205], the National Science Foundation of China [grant number 81872927], the International Partnership Program of Chinese Academy of Sciences [grant number 153631KYSB20160004], the Independent Deployment Program of the Institute of Pharmaceutical Innovation of the Chinese Academy of Sciences [grant number CASIMM0120184005], and the China Postdoctoral Science Foundation [grant number 2019M651623].

Reference

1. Demir M, Lang S and Steffen HM, Nonalcoholic fatty liver disease – current status and future directions. *J Dig Dis* 2015; **16**(10):541-557.
2. Tiniakos DG, Vos MB and Brunt EM, Nonalcoholic fatty liver disease: pathology and pathogenesis. *Annu Rev Pathol* 2010; **5**:145-171.
3. Vernon G, Baranova A and Younossi ZM, Systematic review: the epidemiology and natural history of non-alcoholic fatty liver disease and non-alcoholic steatohepatitis in adults. *Aliment Pharmacol Ther* 2011; **34**(3):274-285.
4. Masarone M, Federico A, Abenavoli L*, et al.*, Non alcoholic fatty liver: epidemiology and natural history. *Rev Recent Clin Trials* 2014; **9**(3):126-133.
5. Alli V and Rogers AM, Gastric bypass and influence on improvement of NAFLD. *Curr Gastroenterol Rep* 2017; **19**:25.
6. Schuppan D and Schattenberg JM, Non-alcoholic steatohepatitis: pathogenesis and novel therapeutic approaches. *J Gastroenterol Hepatol* 2013; **28**(Suppl 1):68-76.
7. Friedman SL, Neuschwander-Tetri BA, Rinella M*, et al.*, Mechanisms of NAFLD development and

therapeutic strategies. *Nat Med* 2018; **24**(7):908-922.

8. Lindenmeyer CC and McCullough AJ, The natural history of nonalcoholic fatty liver disease—an evolving view. *Clin. Liver Dis* 2018; **22**(1):11-21.
9. Mittal S, El-Serag HB, Sada YH*, et al.*, Hepatocellular carcinoma in the absence of cirrhosis in united states veterans is associated with nonalcoholic fatty liver disease. *Clin Gastroenterol Hepatol* 2016; **14**(1):124-131.
10. Buzzetti E, Pinzani M and Tsochatzis EA, The multiple-hit pathogenesis of non-alcoholic fatty liver disease (NAFLD). *Metabolism* 2016; **65**(8):1038-48.
11. Ress C and Kaser S, Mechanisms of intrahepatic triglyceride accumulation. *World J Gastroenterol* 2016; **22**(4):1664-1673.
12. Joost W, Isabel VAP, Michaël M*, et al.*, Strategies, models and biomarkers in experimental nonalcoholic fatty liver disease research. *Prog Lipid Res* 2015; **59**:106-125.
13. Schaap FG, Trauner M and Jansen PLM, Bile acid receptors as targets for drug development. *Nat Rev Gastroenterol Hepatol* 2014; **11**:55-67.
14. Chavez-Talavera O, Tailleux A, Lefebvre P*, et al.*, Bile Acid Control of Metabolism and Inflammation in Obesity, Type 2 Diabetes, Dyslipidemia, and Nonalcoholic Fatty Liver Disease. *Gastroenterology* 2017; **152**(7):1679-1694 e3.
15. Arab JP, Karpen SJ, Dawson PA*, et al.*, Bile acids and nonalcoholic fatty liver disease: Molecular insights and therapeutic perspectives. *Hepatology* 2017; **65**(1):350-362.
16. Hodge RJ and Nunez DJ, The therapeutic potential of TGR5 agonists. Hope or hype. *Diabetes Obes Metab* 2016; **18**:439-443.
17. Mouzaki M, Wang AY, Bandsma R*, et al.*, Bile acids and dysbiosis in non-alcoholic fatty liver disease. *PLoS One* 2016; **11**:e0151829.
18. Kohli R, Myronovych A, Tan BK*, et al.*, Bile acid signaling: mechanism for bariatric surgery, cure for NASH. *Dig Dis* 2015; **33**:440-446.
19. Roberto P, Stefano F, Emidio C*, et al.*, 6r-Ethyl-Chenodeoxycholic Acid (6-ECDCA), a potent and selective FXR agonist endowed with anticholestatic activity. *J Med Chem* 2002; **45**(17):3569-3572.
20. Neuschwander-Tetri BA, Loomba R, Sanyal AJ*, et al.*, Farnesoid X nuclear receptor ligand obeticholic acid for non-cirrhotic, non-alcoholic steatohepatitis (FLINT): a multicentre, randomised, placebo-controlled trial. *Lancet Lond Engl* 2015; **385**(9972):956-965.
21. Pellicciari R, Gioiello A, Macchiarulo A*, et al.*, Discovery of 6alpha-ethyl-23(S)-methylcholic acid (S-EMCA, INT-777) as a potent and selective agonist for the TGR5 receptor, a novel target for diabesity. *J Med Chem* 2009; **52**:7958-7961.
22. Thomas C, Gioiello A, Noriega L*, et al.*, TGR5-mediated bile acid sensing controls glucose homeostasis. *Cell Metab* 2009; **10**(3):167-77.
23. McMahan RH, Wang XX, Cheng LL*, et al.*, Bile acid receptor activation modulates hepatic monocyte activity and improves nonalcoholic fatty liver disease. *J Biol Chem* 2013; **288**:11761-11770.
24. Beraza N, Ofner-Ziegenfuss L, Ehedego H*, et al.*, Nor-ursodeoxycholic acid reverses hepatocyte-specific nemo-dependent steatohepatitis. *Gut* 2011; **60**(3):387-396.
25. Traussnigg S, Schattenberg JM, Demir M*, et al.*, Norursodeoxycholic acid versus placebo in the treatment of non-alcoholic fatty liver disease: a double-blind, randomised, placebo-controlled, phase 2 dose-finding trial. *The Lancet Gastroenterology & Hepatology* 2019; **4**(10):781-793.

26. Wang X-y, Zhang S-y, Li J*, et al.*, Highly lipophilic 3-epi-betulinic acid derivatives as potent and selective TGR5 agonists with improved cellular efficacy. *Acta Pharmacologica Sinica* 2014; **35**(11):1463-1472.
27. Angrish MM, McQueen CA, Cohen-Hubal E*, et al.*, Editor's Highlight: Mechanistic Toxicity Tests Based on an Adverse Outcome Pathway Network for Hepatic Steatosis. *Toxicol Sci* 2017; **159**(1):159-169.
28. Shen L, Hillebrand A, Wang D*, et al.*, Isolation and primary culture of rat hepatic cells. *J Vis Exp* 2012; **29**(64).
29. Kleiner DE, Brunt EM, Van Natta M*, et al.*, Design and validation of a histological scoring system for nonalcoholic fatty liver disease. *Hepatology* 2005; **41**:1313-1321.
30. Roberto P, Gabriele C, Emidio C*, et al.*, Bile acid derivatives as ligands of the farnesoid X receptor. synthesis, evaluation, and structure-activity relationship of a series of body and side chain modified analogues of chenodeoxycholic acid. *J Med Chem* 2004; **47**:4559-4569.
31. Roberto P, Antimo G, Gabriele C*, et al.*, Back door modulation of the farnesoid X receptor: design, synthesis, and biological evaluation of a series of side chain modified chenodeoxycholic acid derivatives. *J Med Chem* 2006; **49**:4208-4215.
32. Xiao H, Li P, Li X*, et al.*, Synthesis and biological evaluation of a series of bile acid derivatives as FXR agonists for treatment of NASH. *ACS Med Chem Lett* 2017; **8**:1246-1251.
33. Nishimaki-Mogami T, Une M, Fujino T*, et al.*, Identification of intermediates in the bile acid synthetic pathway as ligands for the farnesoid X receptor. *J Lipid Res* 2004; **45**:1538-1545.
34. Hiroyuki S, Antonio M, Charles T*, et al.*, Novel potent and selective bile acid derivatives as TGR5 agonists: biological screening, structure-activity relationships, and molecular modeling studies. *J Med Chem* 2008; **51**:1831-1841.
35. Byrne CD and Targher G, NAFLD: a multisystem disease. *J. Hepatol* 2015; **62**(1 Suppl):S47-S64.
36. Begriche K, Igoudjil A, Pessayre D*, et al.*, Mitochondrial dysfunction in NASH: Causes, consequences and possible means to prevent it. *Mitochondrion* 2006; **6**(1):1-8.
37. Perino A and Schoonjans K, TGR5 and immunometabolism: insights from physiology and pharmacology. *Trends Pharmacol Sci* 2015; **36**(12):847-857.
38. Luckert C, Braeuning A, de Sousa G*, et al.*, Adverse Outcome Pathway-Driven Analysis of Liver Steatosis in Vitro: A Case Study with Cyproconazole. *Chem Res Toxicol* 2018; **31**(8):784-798.
39. Pols TW, Nomura M, Harach T*, et al.*, TGR5 activation inhibits atherosclerosis by reducing macrophage inflammation and lipid loading. *Cell Metab* 2011; **14**(6):747-57.
40. Wang YD, Chen WD, Yu D*, et al.*, The G-protein-coupled bile acid receptor, Gpbar1 (TGR5), negatively regulates hepatic inflammatory response through antagonizing nuclear factor kappa light-chain enhancer of activated B cells (NF-kappaB) in mice. *Hepatology* 2011; **54**(4):1421-32.
41. Watanabe M, Houten SM, Wang L*, et al.*, Bile acids lower triglyceride levels via a pathway involving FXR, SHP, and SREBP-1c. *J Clin Invest* 2004; **113**:1408-1418.
42. Carr RM and Reid AE, FXR agonists as therapeutic agents for non-alcoholic fatty liver disease. *Curr Atheroscler Rep* 2015; **17**(4):500-516.
43. Buqué X, Cano A, Miquilena-Colina ME*, et al.*, High insulin levels are required for FAT/CD36 plasma membrane translocation and enhanced fatty acid uptake in obese Zucker rat hepatocytes. *Am. J. Physiol. Endocrinol. Metab* 2012; **303**:E504-E514.
44. Miquilena-Colina ME, Lima-Cabello E, Sánchez-Campos S*, et al.*, Hepatic fatty acid translocase

CD36 upregulation is associated with insulin resistance, hyperinsulinaemia and increased steatosis in non-alcoholic steatohepatitis and chronic hepatitis C. *Gut* 2011; **60**(10):1394-1402.

45. Greco D, Kotronen A, Westerbacka J*, et al.*, Gene expression in human NAFLD. *Am. J. Physiol. Gastrointest. Liver Physiol* 2008; **294**:G1281-G1287.
46. Wilson CG, Tran JL, Erion DM*, et al.*, Hepatocyte-Specific Disruption of CD36 Attenuates Fatty Liver and Improves Insulin Sensitivity in HFD-Fed Mice. *Endocrinology* 2016; **157**(2):570-85.
47. Jung HL, Jie Z and Wen X, PXR and LXR in hepatic steatosis: a new dog and an old dog with new tricks. *Mol Pharm* 2007; **5**(1):60-66.
48. Nie B, Park HM, Kazantzis M*, et al.*, Specific bile acids inhibit hepatic fatty acid uptake in mice. *Hepatology* 2012; **56**(4):1300-10.
49. Ibrahimi A, Bonen A, Blinn WD*, et al.*, Muscle-specific overexpression of FAT/CD36 enhances fatty acid oxidation by contracting muscle, reduces plasma triglycerides and fatty acids, and increases plasma glucose and insulin. *J Biol Chem* 1999; **274**(38):. 6761-26766.
50. Kim J, Yang G, Kim Y*, et al.*, AMPK activators: mechanisms of action and physiological activities. *Exp Mol Med* 2016; **48**:e224.
51. Woods A, Williams JR, Muckett PJ*, et al.*, Liver-specific activation of AMPK prevents steatosis on a high-fructose diet. *Cell Rep* 2017; **18**(13):3034-3051.
52. Yamada E, Pessin JE, Kurland IJ*, et al.*, Fyn-dependent regulation of energy expenditure and body weight is mediated by tyrosine phosphorylation of LKB1. *Cell Metab* 2010; **11**(2):113-124.
53. Zhao L, Zhang C, Luo X*, et al.*, CD36 palmitoylation disrupts free fatty acid metabolism and promotes tissue inflammation in non-alcoholic steatohepatitis. *J Hepatol* 2018; **69**(3):705-717.

Figure legends

Scheme 1. Synthesis of A17. Cat. catalyst, DCM dichloromethane, HATU 2-(7-Azabenzotriazol-1-yl)-N, N, N', N'-tetramethyluronium hexafluorophosphate, r.t. room temperature, TEA triethylamine, THF tetrahydrofuran, UDCA ursodesoxycholic acid.

Fig. 1. Intracellular TG concentrations were up-regulated by OA in RPHs, while A17 ameliorated the elevation, improved cell viability and decreased lipid peroxidation. Cells were treated with various concentrations of OA for 24 h. Corresponding concentrations of BSA were used as negative controls. (A) Cell viability was measured by CCK-8 assay and the cells were harvested for intracellular TG measurement (B). Then, 500 μM OA was used to induce

steatosis in RPHs. Cells induced by OA were incubated with 10 or 25 μM A17 for 24 h. OCA served as the positive control. After treatment, the cytotoxicity of A17 was tested via CCK-8 assay (C). Intracellular TG (D) and MDA (E) were measured to investigate the effect of A17 on lipid accumulation and peroxidation respectively. MDA malondialdehyde, OA oleic acid, OCA obeticholic acid, RPHs rat primary hepatocytes, TG triglyceride. Values were expressed as the mean ± SD, $n = 3$, #$P < 0.05$, ##$P < 0.01$, ###$P < 0.001$ versus the vehicle group; *$P < 0.05$, **$P < 0.01$, ***$P < 0.001$ versus the OA group. The Student's t test was used to precede the comparison between two groups, and One-way ANOVA was used in case of multiple testing.

Fig. 2. A17 reduced the uptake of FA in RPHs via inhibiting the protein expression of Cd36. RPHs were treated with 500 μM OA and 25 μM A17 or OCA for 24 h. Triacsin C served as positive control (incubated with cells for 2 h). (A) FA uptake was assessed by adding fluorescent fatty acid analog and detected for 30 min. (B) The protein expression of Fabp(pm), Fatp2, Fatp5 and Cd36 in RPHs were determined by western blot and were normalized against Gapdh. Cd36 fatty acid translocase, FA fatty acid, Fabp(pm) fatty acid binding protein (plasma membrane), Fatp2 fatty acid transport protein 2, Fatp5 fatty acid transport protein 5, OA oleic acid, OCA obeticholic acid. Values were expressed as the mean ± SD, $n = 3$ or 4, **$P < 0.01$, ***$P < 0.001$ versus the OA group. One-way ANOVA was used to test statistical significance.

Fig. 3. A17 elevated the oxidation of FA in RPHs via increasing the phosphorylation of

AMPKα/ACC/Cpt-1α pathway. RPHs were treated with 500 μM OA and 25 μM A17 or OCA for 24 h, 50 μM amiodarone was used as positive control. (A) OCR of cells was assessed using the Seahorse Flux Analyzer XFe96 FAO assay and the maximal respiration was analyzed to identify the effect of A17 and OCA on mitochondrial respiration. (B) The protein expression levels of total and phosphorylated AMPKα, total and phosphorylated ACC and Cpt-1α in RPHs, Gapdh served as the loading control. (C) The mRNA expression of Cpt-1α in RPHs normalized against Gapdh. In inhibitor experiment, RPHs were pretreated with 10 μM Etomoxir for 24 h and then with 500 μM OA, 25 μM A17 and 10 μM Etomoxir for another 24 h. Intracellular TG (D) and cell viability (E) were measured to investigate whether Cpt-1α inhibition can block the effects of A17 on OA-induced RPHs. ACC acetyl-CoA carboxylase, AMPKα adenosine monophosphate (AMP)-activated protein kinase alpha, A/R antimycin/rotenone, Cpt-1α carnitine palmitoyltransferase-1α, FAO fatty acid oxidation, OA oleic acid, OCA obeticholic acid, OCR oxygen consumption rate, oligo oligomycin, TG triglyceride. Values were expressed as the mean ± SD, n = 3 or 6, ###P < 0.001 versus the vehicle group; *P < 0.05, **P < 0.01, ***P < 0.001 versus the OA group; ΔP < 0.05, ΔΔΔP < 0.001 versus the OA + A17 group. One-way ANOVA was used to test statistical significance.

Fig. 4. A17 inhibited inflammatory response in Raw264.7 by activating TGR5. (A) Binding potencies of OCA and A17 to FXR. Response are expressed as percent of the activity of 50 μM of OCA. (B) Activities of INT-777 and A17 on TGR5 in HEK293 cells transiently transfected with human TGR5 expression vector were evaluated using a cyclic-AMP assay. Response are expressed as percent of the activity of 100 μM of INT-777. (C) The

concentrations of NO, TNF-α and IL-6 in the supernatant of Raw264.7 cells incubated with 1 μg/mL LPS and 25 μM A17 or 10 μM Dex for 8 h. (D) The protein expression levels of total and phosphorylated IκBα in Raw264.7 cells incubated with 1 μg/mL LPS and 25 μM A17 or INT-777 for 1 h. Gapdh served as the loading control. Dex dexamethasone, IκBα nuclear factor of kappa light polypeptide gene enhancer in B-cells inhibitor alpha, IL-6 interleukin-6, LPS lipopolysaccharide, NO nitric oxide, OA oleic acid, OCA obeticholic acid, TGR5 Takeda G-protein-coupled receptor 5, TNF-α tumor necrosis factor alpha. Values were expressed as the mean ± SD, $n = 3$, ###$P < 0.001$ versus the vehicle group; *$P < 0.05$, **$P < 0.01$, ***$P < 0.001$ versus the OA group or LPS group. One-way ANOVA was used to test statistical significance.

Fig. 5. A17 administration markedly improved steatosis and inflammation in HF-induced hamsters. Hamsters were divided into five groups as follows. Vehicle group, standard diet + vehicle, A17 group, standard diet + A17, HF group, HF diet + vehicle, HF + OCA group and HF + A17 group. After feeding with HF or standard diet for 16 weeks, the hamsters were administrated with drugs for another 6 weeks. (A) Body weight changes of hamsters during HF feeding and drug treatment. (B) Representative pictures of liver histology changes in H & E and Oil Red staining (magnification × 20). (C) Inflammation and steatosis scores of liver histology changes. H & E hematoxylin and eosin, HF high fat, OCA obeticholic acid. Values were expressed as the mean ± SD, $n = 5$, ###$P < 0.001$ versus the vehicle group; *$P < 0.05$, **$P < 0.01$, ***$P < 0.001$ versus the HF group. One-way ANOVA was used to test statistical significance.

Fig. 6. A17 alleviated NASH via AMPKα/ACC/Cpt-1α pathway, inhibiting Cd36 and activating TGR5. (A) The protein expression levels of Fabp(pm), Fatp2, Fatp5 and Cd36 in hamster liver samples, β-actin served as the loading control. (B) The protein expression levels of total and phosphorylated AMPKα, total and phosphorylated ACC and Cpt-1α in hamster liver samples were normalized against β-actin. (C) The mRNA expression of Cpt-1α in hamster liver samples, normalized against Gapdh. (D) The protein expression levels of total and phosphorylated IκBα and IL-6 in hamster liver samples, β-actin served as the loading control. ACC acetyl-CoA carboxylase, AMPKα adenosine monophosphate (AMP)-activated protein kinase alpha, Cd36 fatty acid translocase, Cpt-1α carnitine palmitoyltransferase-1α, Fabp(pm) fatty acid binding protein (plasma membrane), Fatp2 fatty acid transport protein 2, Fatp5 fatty acid transport protein 5, HF high fat, IκBα nuclear factor of kappa light polypeptide gene enhancer in B-cells inhibitor alpha, IL-6 interleukin-6, NASH non-alcoholic steatohepatitis, Values were expressed as the mean ± SD, $n = 3$, ##$P < 0.01$, ###$P < 0.001$ versus the vehicle group, *$P < 0.05$, **$P < 0.01$, ***$P < 0.001$ versus the HF group. One-way ANOVA was used to test statistical significance.

Fig. 7. A17 had three pharmacological effects on NASH. First, A17 reduced the Cd36 expression in hepatocytes, suppressing FA uptake into the liver. Second, A17 stimulated the phosphorylation of AMPKα and ACC and enhanced the expression of Cpt-1α, promoting FA oxidation in hepatocytes. Third, A17 activated TGR5 on Kupffer cells, increasing cAMP levels and blunting the phosphorylation of IκBα, which led to the inhibition of inflammatory

response. ACC acetyl-CoA carboxylase, AMPKα adenosine monophosphate (AMP)-activated protein kinase alpha, cAMP, cyclic-AMP, Cd36 fatty acid translocase, Cpt-1α carnitine palmitoyltransferase-1α, FA fatty acid, IκBα nuclear factor of kappa light polypeptide gene enhancer in B-cells inhibitor alpha, NASH non-alcoholic steatohepatitis, TGR5 Takeda G-protein-coupled receptor 5.

Supplemental figure legends

Fig. S1. A17 could enter into RPHs. After treated with 10, 25 or 50 μM A17 for 24 h, RPHs were collected and intracellular A17 was measured using HPLC-MS. RPHs rat primary hepatocytes. Values were expressed as the mean ± SD, $n = 3$.

Fig. S2. Intracellular TG concentrations were significantly decreased by 25 μM OCA in OA-induced RPHs. RPHs induced by 500 μM OA were incubated with 0.01, 0.1, 1, 10 or 25 μM OCA for 24 h. Intracellular TG were measured to investigate the effect of OCA on lipid accumulation. OA oleic acid, OCA obeticholic acid, RPHs rat primary hepatocytes, TG triglyceride. Values were expressed as the mean ± SD, $n = 3$, ###$P < 0.001$ versus the vehicle group; *$P < 0.05$ versus the OA group. One-way ANOVA was used to test statistical significance.

Fig. S3. Neither in OA-induced RPHs nor in HF-induced hamsters could A17 affect the expression of FXR target genes. (A) The mRNA expression levels of Shp, Cyp7a1 and Bsep

in RPHs treated with 500 μM OA and 25 μM A17 or OCA for 24 h. Gapdh served as the loading control. (B) The mRNA expression levels of Shp, Cyp7a1 and Bsep in hamsters treated with vehicle, 20 mg/kg OCA or 50 mg/kg A17 for 6 weeks after been fed HF diet for 16 weeks. Gapdh served as the loading control. Bsep bile salt export pump, Cyp7a1 cytochrome P450 7a1, FXR farnesoid X receptor, HF high fat, OA oleic acid, OCA obeticholic acid, RPHs rat primary hepatocytes, Shp small heterodimer partner, Values were expressed as the mean ± SD, $n = 3$, $^{*}P < 0.05$, $^{**}P < 0.01$, $^{***}P < 0.001$ versus the OA group or the HF group. One-way ANOVA was used to test statistical significance.

Fig. S4. Neither cell viability nor intracellular TG concentrations were affected by INT-777 in OA-induced RPHs. RPHs induced by 500 μM OA were incubated with 10, 25 or 50 μM INT-777 for 24 h. 25 μM A17 served as the positive control. Cell viability (A) and intracellular TG (B) were measured to investigate the effect of INT-777 on lipid accumulation. OA oleic acid, RPHs rat primary hepatocytes, TG triglyceride. Values were expressed as the mean ± SD, $n = 3$, $^{\#\#}P < 0.01$ versus the vehicle group; $^{*}P < 0.05$, $^{***}P < 0.001$ versus the OA group. One-way ANOVA was used to test statistical significance.

Fig. S5. OCA administration at 30 mg/kg markedly exacerbated liver injuries in HF-induced hamsters. Hamsters were divided into four groups as follows. Vehicle group, standard diet + vehicle, HF group, HF diet + vehicle, HF + 30 mg/kg OCA group and HF + 50 mg/kg A17 group. After feeding with HF or standard diet for 16 weeks, the hamsters were administrated with drugs for another 2 weeks. Serum ALT (A), AST (B) and TBIL (C) levels were measured.

ALT alanine aminotransferase, AST aspartate aminotransferase, HF high fat, OCA obeticholic acid, TBIL, total bilirubin. Values were expressed as the mean ± SD, $n = 5$, #$P < 0.05$, ##$P < 0.01$ versus the vehicle group; **$P < 0.01$, *** $P < 0.001$ versus the HF group. One-way ANOVA was used to test statistical significance.

Credit Author Statement

Ying Wang, Guoyu Pan, Junxing Niu and Lijiang Xuan designed the research; Ying Wang, Yao Zhu, Qiangqiang Deng, Shimeng Guo, Haowen Jiang, Zhaoliang Peng, Yaru Xue conducted the experiments; Ying Wang, Shimeng Guo, Haowen Jiang and Zhaoliang Peng were responsible for the data analysis; Ying Wang and Guoyu Pan wrote the manuscript; Yao Zhu, Shimeng Guo, Huige Peng and Lijiang Xuan helped revise the manuscript. All the authors reviewed and agreed on the final version.

Declaration of interests

☒ The authors declare that they have no known competing financial interests or personal relationships that could have appeared to influence the work reported in this paper.

☐The authors declare the following financial interests/personal relationships which may be considered as potential competing interests:

Declarations of interest: none

Tables

Table 1. Primer pairs for real-time PCR experiments.

Target gene	Direction	Primer sequence (5'-3')
Rat		
Bsep	Forward	TGGAAAGGAATGGTGATGGG
	Reverse	CAGAAGGCCAGTGCATAACAGA
Cpt-1α	Forward	AGGTCTGGCTCTACCACGAT
	Reverse	CACTCTGTCTGCAGCAGTGA
Cyp7a1	Forward	CACCATTCCTGCAACCTTTT
	Reverse	GTACCGGCAGGTCATTCAGT
Shp	Forward	GGCACTATCCTCTTCAACCCA
	Reverse	TCCAGGACTTCACACAATGCC
Gapdh	Forward	AGGTCGGTGTGAACGGATTTG
	Reverse	GGGGTCGTTGATGGCAACA
Hamster		
Bsep	Forward	AGGGCTCTCAACTCTCTCG
	Reverse	ATACAGGTCCGAGCCTCTCTG
Cpt-1α	Forward	CTCAGTGGGACTCGACTCTTCA
	Reverse	GGCCTCTCTCTCTACACGACAA
Cyp7a1	Forward	TTCCTGCAACCTTCTGGAGC
	Reverse	GCCTCCTTCATGATGCTATCTAGT
Shp	Forward	AGGGAGGCCTTGGATGTC
	Reverse	AGAAGCACGGCAGGTTCC
Gapdh	Forward	GAAGATCATCCCTGCATCCA
	Reverse	CCAGTGAGCTTCCCGTTCA

Bsep bile salt export pump, Cpt-1α carnitine palmitoyltransferase-1α, Cyp7a1 cytochrome P450 7a1, Shp, short heterodimer partner.

Table 2. Hamster serum and liver biochemical analysis

	Vehicle	A17	HF	HF + OCA	HF + A17
Serum					
TG (mM)	1.17±0.27	1.01±0.09	3.11±0.19$^{###}$	1.65±0.27***	1.57±0.36***
TC (mM)	4.57±0.29	4.71±0.67	6.50±0.75$^{##}$	6.65±1.44	4.8±0.91*
LDL-C (mM)	1.29±0.20	1.06±0.12	2.11±0.27$^{##}$	1.85±0.59	1.43±0.46*
ALT (U/L)	7.86±2.59	13.09±4.44	85.52±32.14$^{###}$	39.10±9.98**	21.20±5.79***

AST (U/L)	1.19±0.11	3.23±2.71	37.40±13.79$^{###}$	14.40±4.80**	5.54±2.76***
Liver					
TG (mM)	4.01±0.53	3.83±0.66	6.29±0.74$^{##}$	3.15±0.59***	3.27±0.81***
TC (mM)	7.22±0.40	6.82±0.74	12.11±1.55$^{##}$	9.75±2.18	10.58±2.50

ALT alanine aminotransferase, AST aspartate aminotransferase, HF high fat, LDL-C low density lipoprotein cholesterol, OCA obeticholic acid, TC total cholesterol, TG triglyceride. Values were expressed as the mean ± SD, $n = 5$, #$P < 0.05$, ##$P < 0.01$, ###$P < 0.001$ versus the vehicle group; *$P < 0.05$, **$P < 0.01$, *** $P < 0.001$ versus the HF group. One way ANOVA was used to test statistical significance.

Highlights

- A novel bile acid analog A17 was synthesized to treat NASH in hamsters
- A17 activated TGR5 and ameliorated inflammation in liver
- A17 reduced lipid uptake by inhibiting Cd36 expression in hepatocytes
- A17 promoted lipid oxidation by activating AMPK pathway in hepatocytes
- A17 had wider safety window compared with OCA

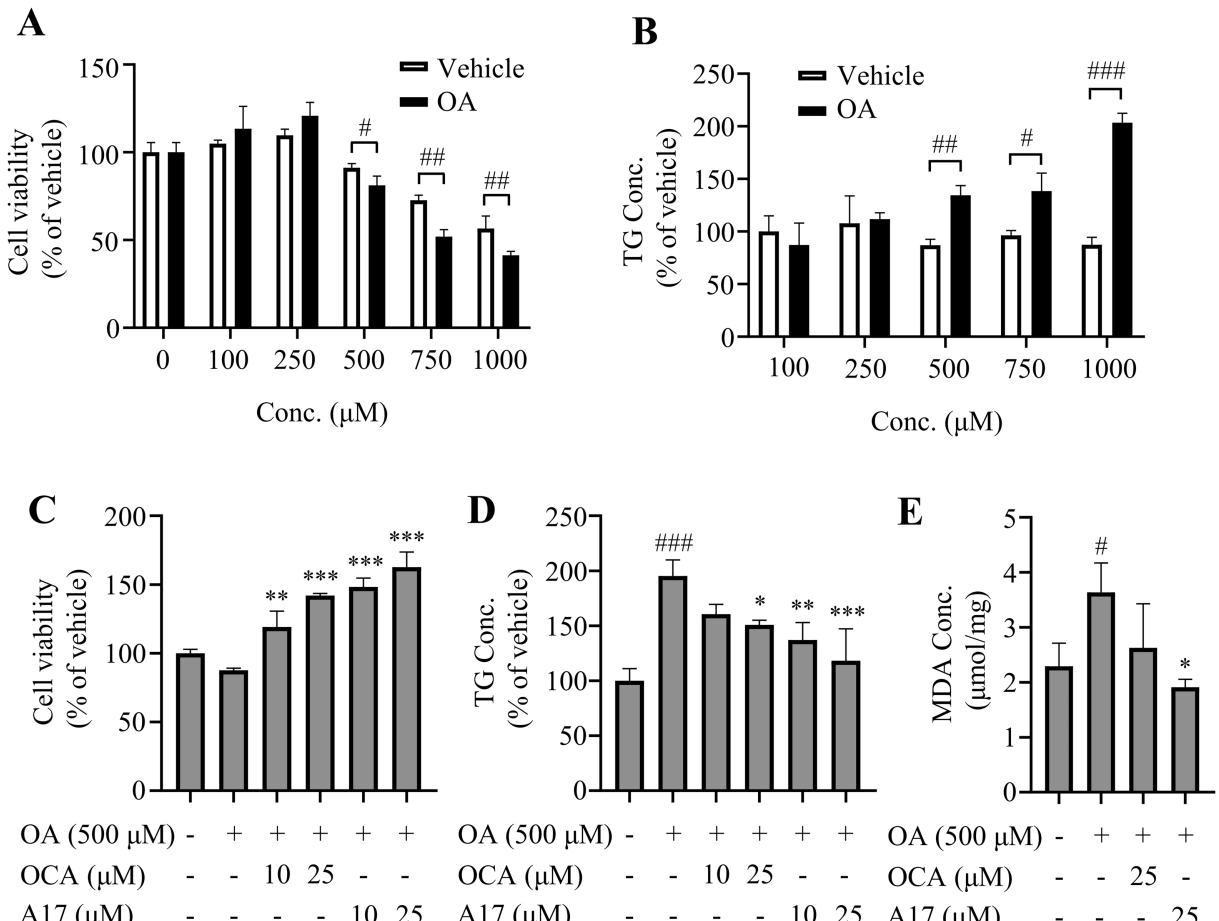
A
Cell viability (% of vehicle)
Vehicle
OA
Conc. (μM)
B
TG Conc. (% of vehicle)
Vehicle
OA
Conc. (μM)
C
Cell viability (% of vehicle)
OA (500 μM)
OCA (μM)
A17 (μM)
D
TG Conc. (% of vehicle)
OA (500 μM)
OCA (μM)
A17 (μM)
E
MDA Conc. (μmol/mg)
OA (500 μM)
OCA (μM)
A17 (μM)

Figure 1

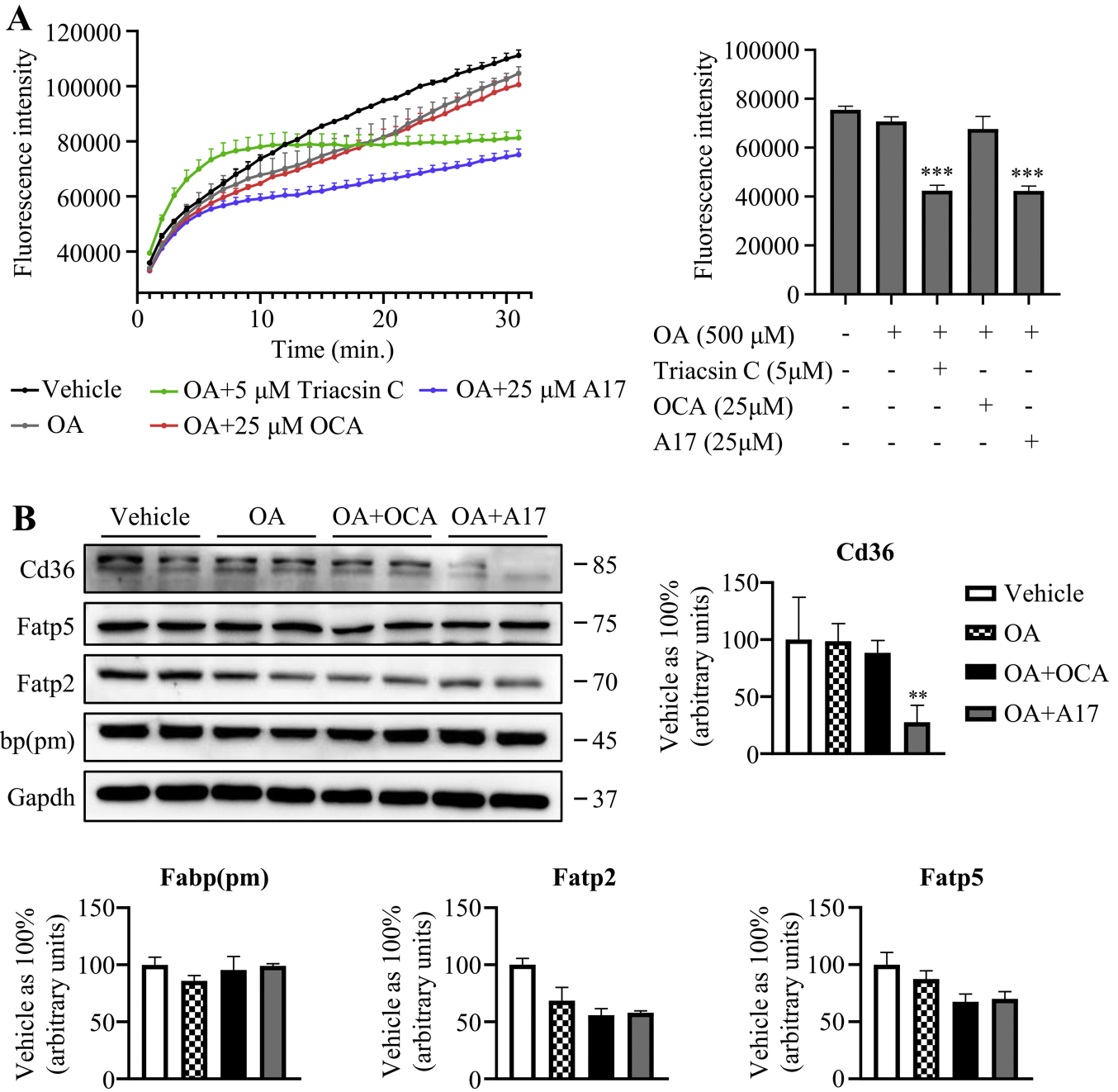
A
Fluorescence intensity
120000
100000
80000
60000
40000
0
10
20
30
Time (min.)
Vehicle
OA
OA+5 μM Triacsin C
OA+25 μM OCA
OA+25 μM A17
Fluorescence intensity
100000
80000
60000
40000
20000
0
***
***
OA (500 μM) - + + + +
Triacsin C (5μM) - - + - -
OCA (25μM) - - - + -
A17 (25μM) - - - - +
B
Vehicle
OA
OA+OCA
OA+A17
Cd36
Fatp5
Fatp2
Fabp(pm)
Gapdh
85
75
70
45
37
Cd36
Vehicle as 100% (arbitrary units)
150
100
50
0
**
Vehicle
OA
OA+OCA
OA+A17
Fabp(pm)
Fatp2
Fatp5

Figure 2

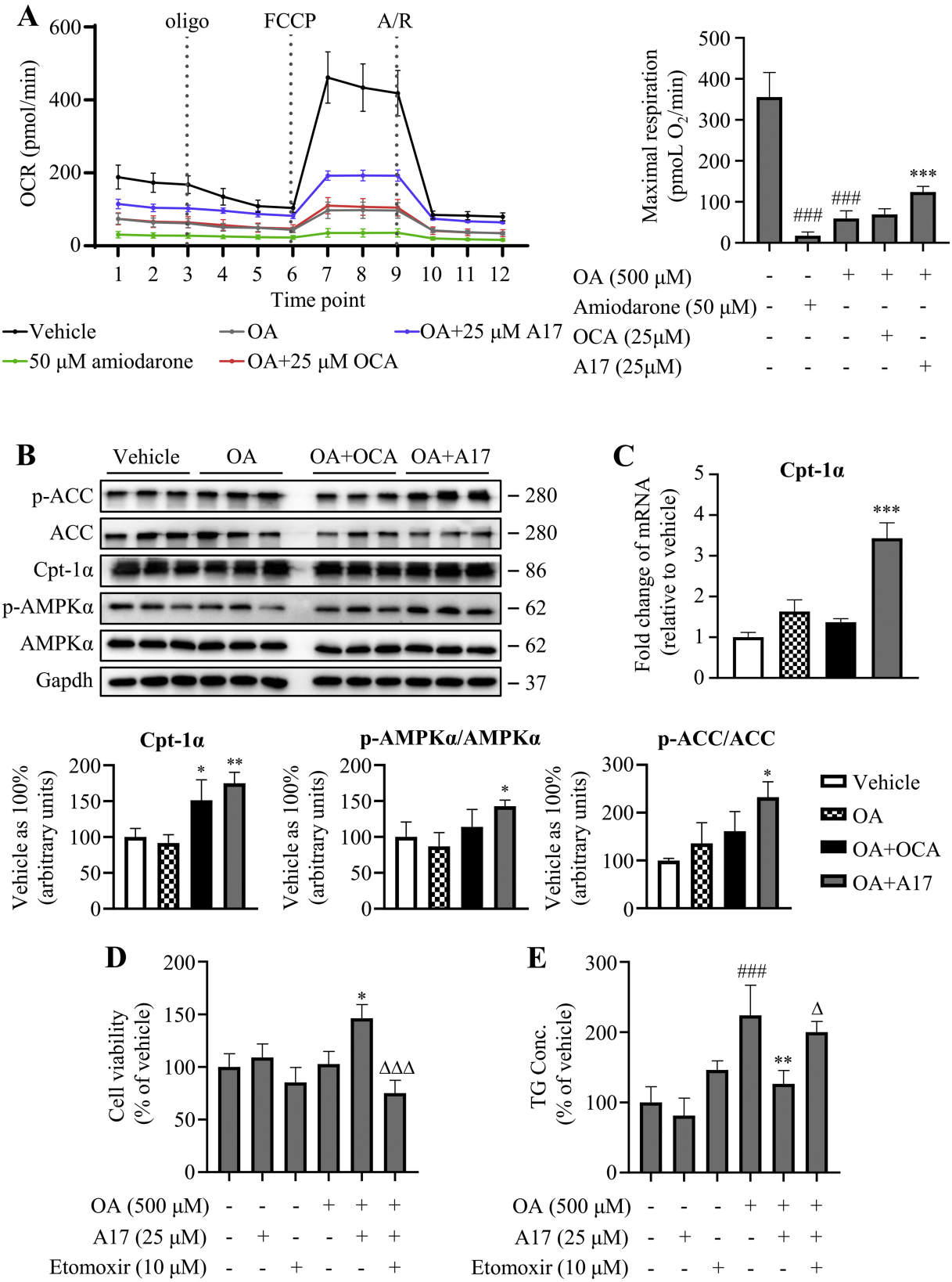
A
oligo
FCCP
A/R
OCR (pmol/min)
Time point
Vehicle
OA
OA+25 μM A17
50 μM amiodarone
OA+25 μM OCA
Maximal respiration (pmoL O2/min)
OA (500 μM)
Amiodarone (50 μM)
OCA (25μM)
A17 (25μM)
B
Vehicle
OA
OA+OCA
OA+A17
p-ACC
ACC
Cpt-1α
p-AMPKα
AMPKα
Gapdh
C
Cpt-1α
Fold change of mRNA (relative to vehicle)
Cpt-1α
p-AMPKα/AMPKα
p-ACC/ACC
Vehicle as 100% (arbitrary units)
Vehicle
OA
OA+OCA
OA+A17
D
Cell viability (% of vehicle)
OA (500 μM)
A17 (25 μM)
Etomoxir (10 μM)
E
TG Conc. (% of vehicle)
OA (500 μM)
A17 (25 μM)
Etomoxir (10 μM)

Figure 3

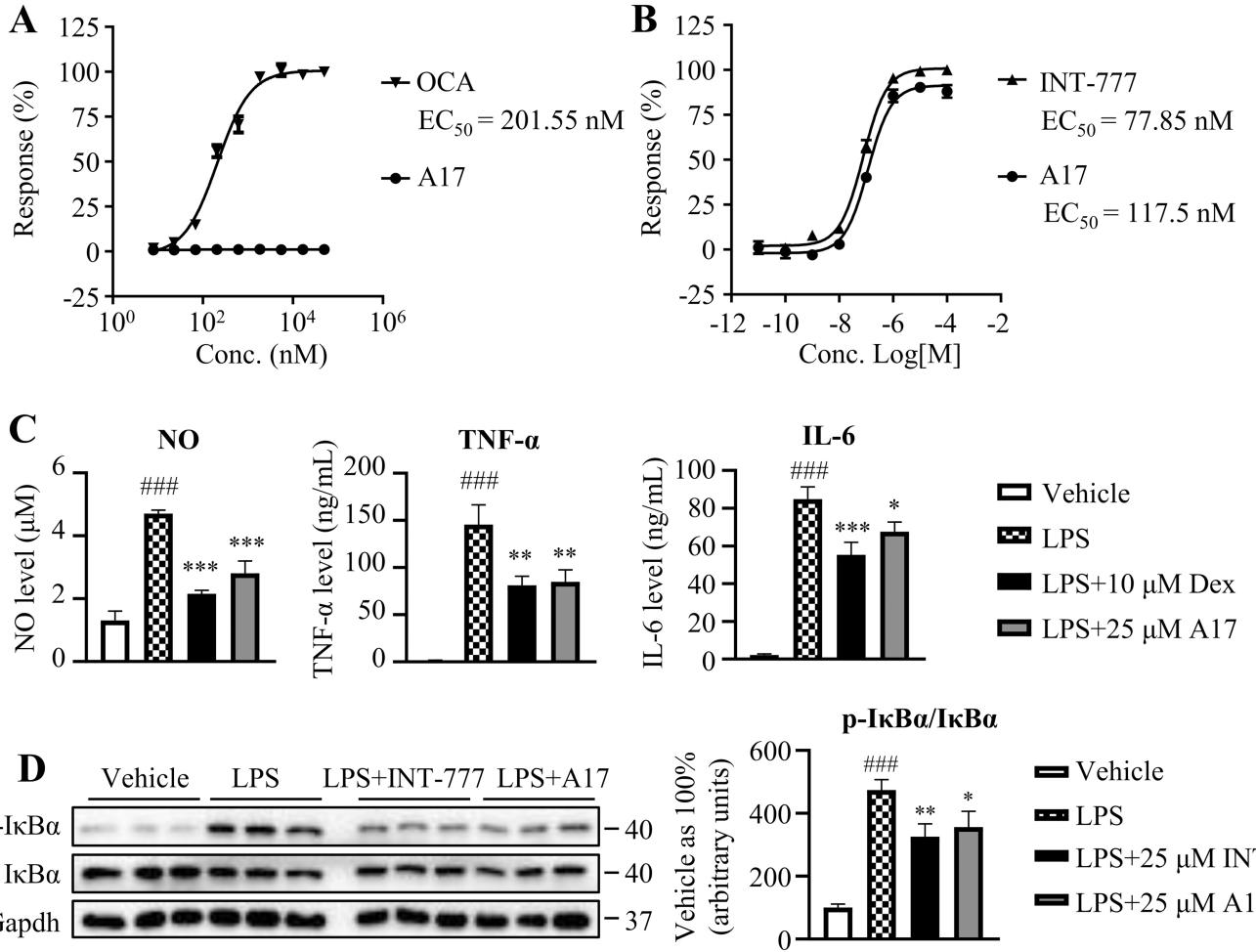
A
Response (%)
Conc. (nM)
OCA
EC50 = 201.55 nM
A17
B
Response (%)
Conc. Log[M]
INT-777
EC50 = 77.85 nM
A17
EC50 = 117.5 nM
C
NO
NO level (μM)
TNF-α
TNF-α level (ng/mL)
IL-6
IL-6 level (ng/mL)
Vehicle
LPS
LPS+10 μM Dex
LPS+25 μM A17
D
Vehicle
LPS
LPS+INT-777
LPS+A17
p-IκBα
IκBα
Gapdh
p-IκBα/IκBα
Vehicle as 100% (arbitrary units)
Vehicle
LPS
LPS+25 μM INT-777
LPS+25 μM A17

Figure 4

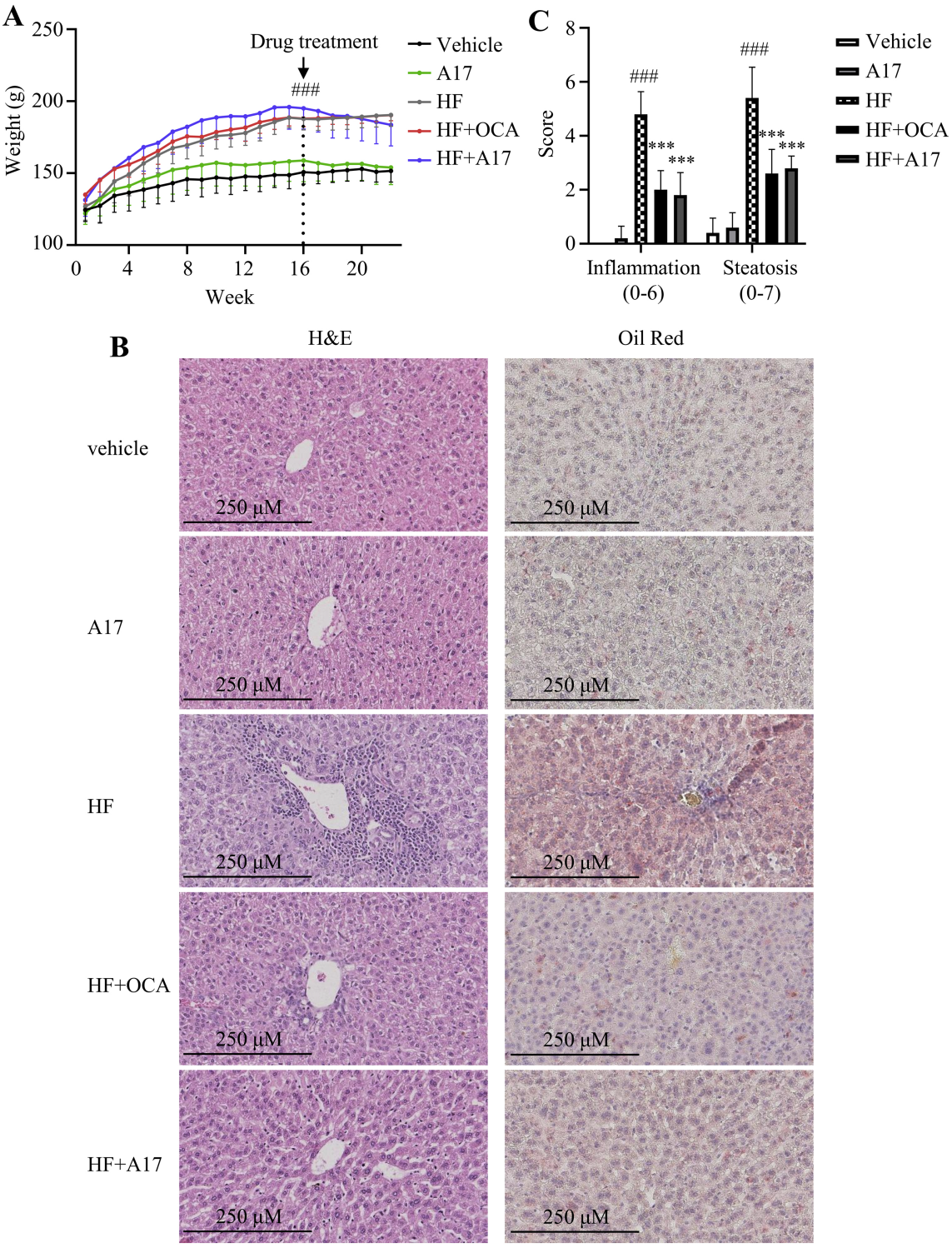
A
Weight (g)
250
200
150
100
0
4
8
12
16
20
Week
Drug treatment
###
Vehicle
A17
HF
HF+OCA
HF+A17
C
Score
8
6
4
2
0
###
###
***
***
***
***
Inflammation
(0-6)
Steatosis
(0-7)
Vehicle
A17
HF
HF+OCA
HF+A17
B
H&E
Oil Red
vehicle
A17
HF
HF+OCA
HF+A17
250 μM

Figure 5

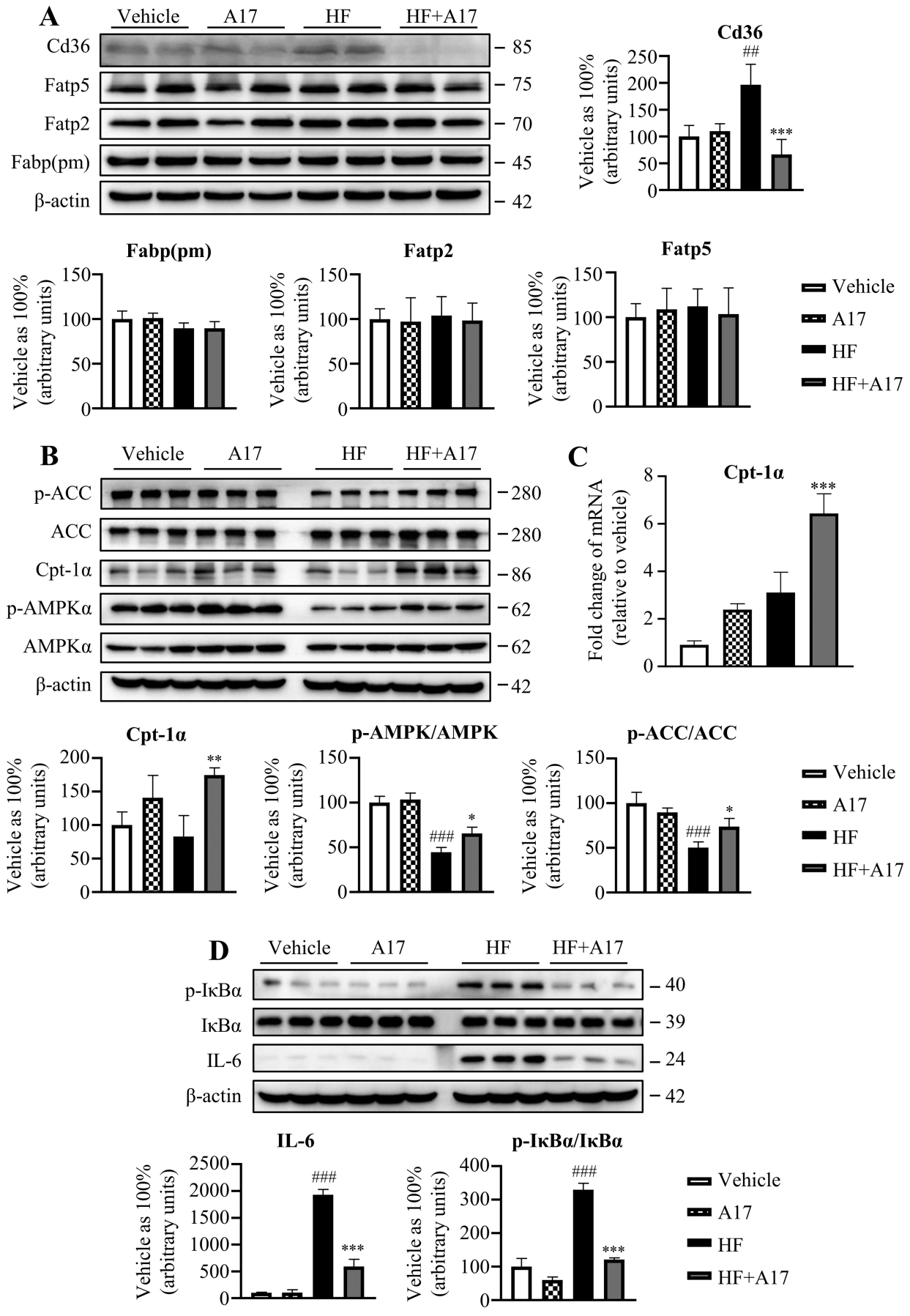
A
Vehicle
A17
HF
HF+A17
Cd36
Fatp5
Fatp2
Fabp(pm)
β-actin
85
75
70
45
42
Cd36
Fabp(pm)
Fatp2
Fatp5
Vehicle as 100% (arbitrary units)
##
***
Vehicle
A17
HF
HF+A17
B
p-ACC
ACC
Cpt-1α
p-AMPKα
AMPKα
β-actin
280
280
86
62
62
42
C
Cpt-1α
Fold change of mRNA (relative to vehicle)
***
p-AMPK/AMPK
p-ACC/ACC
**
###
*
D
p-IκBα
IκBα
IL-6
β-actin
40
39
24
42
IL-6
p-IκBα/IκBα

Figure 6

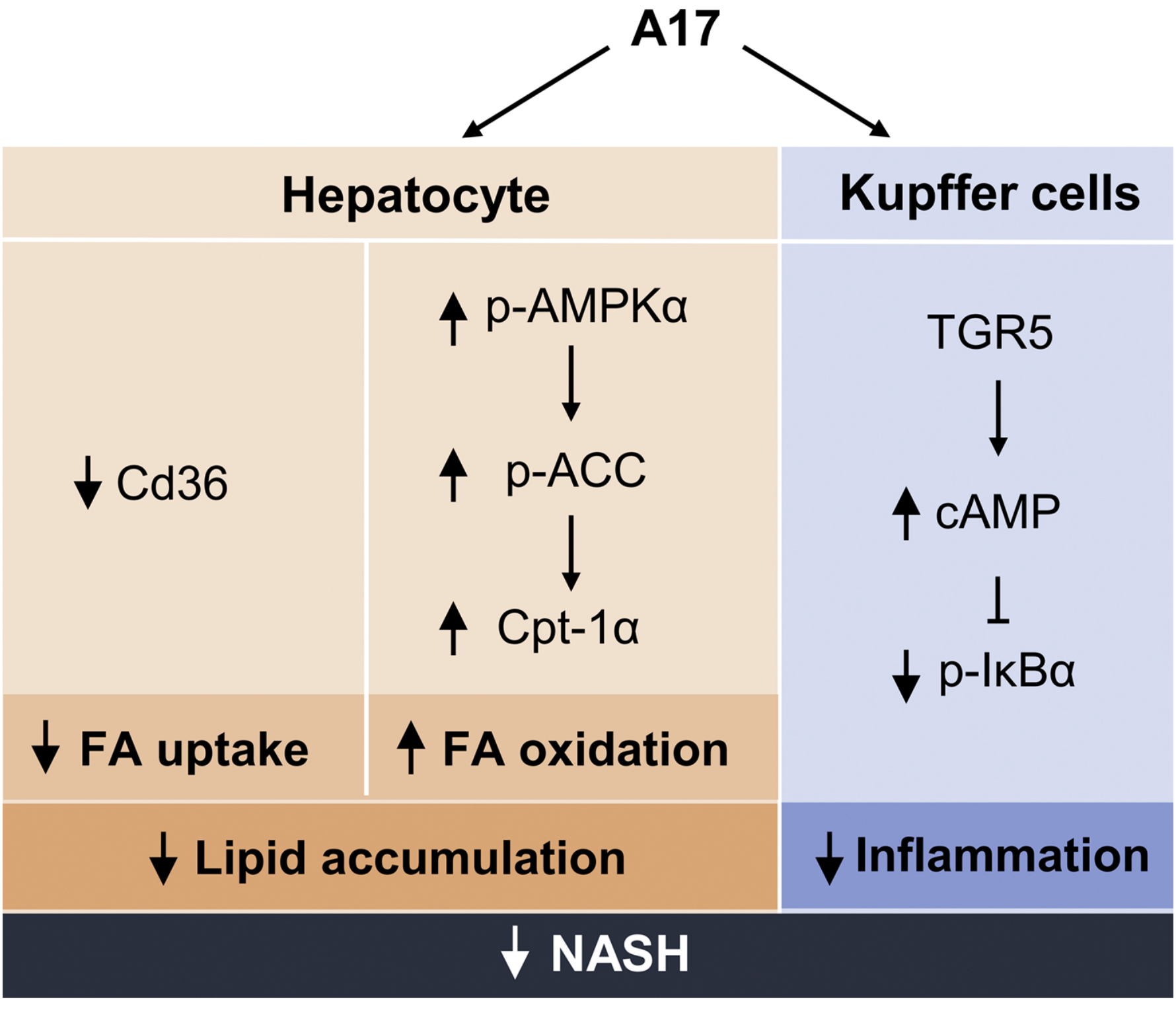
A17
Hepatocyte
Kupffer cells
Cd36
p-AMPKα
p-ACC
Cpt-1α
TGR5
cAMP
p-IκBα
FA uptake
FA oxidation
Lipid accumulation
Inflammation
NASH

Figure 7

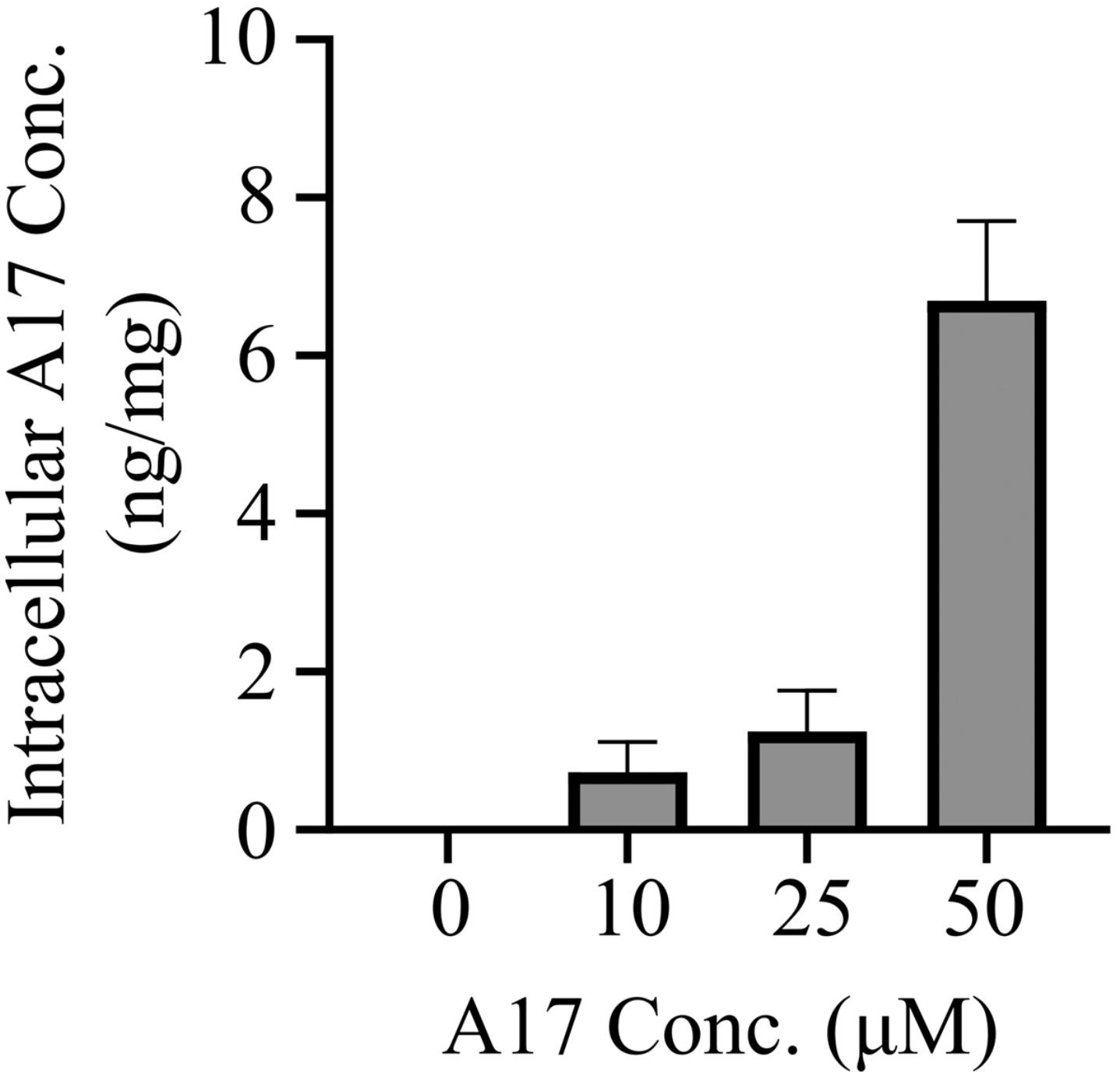

Figure 8

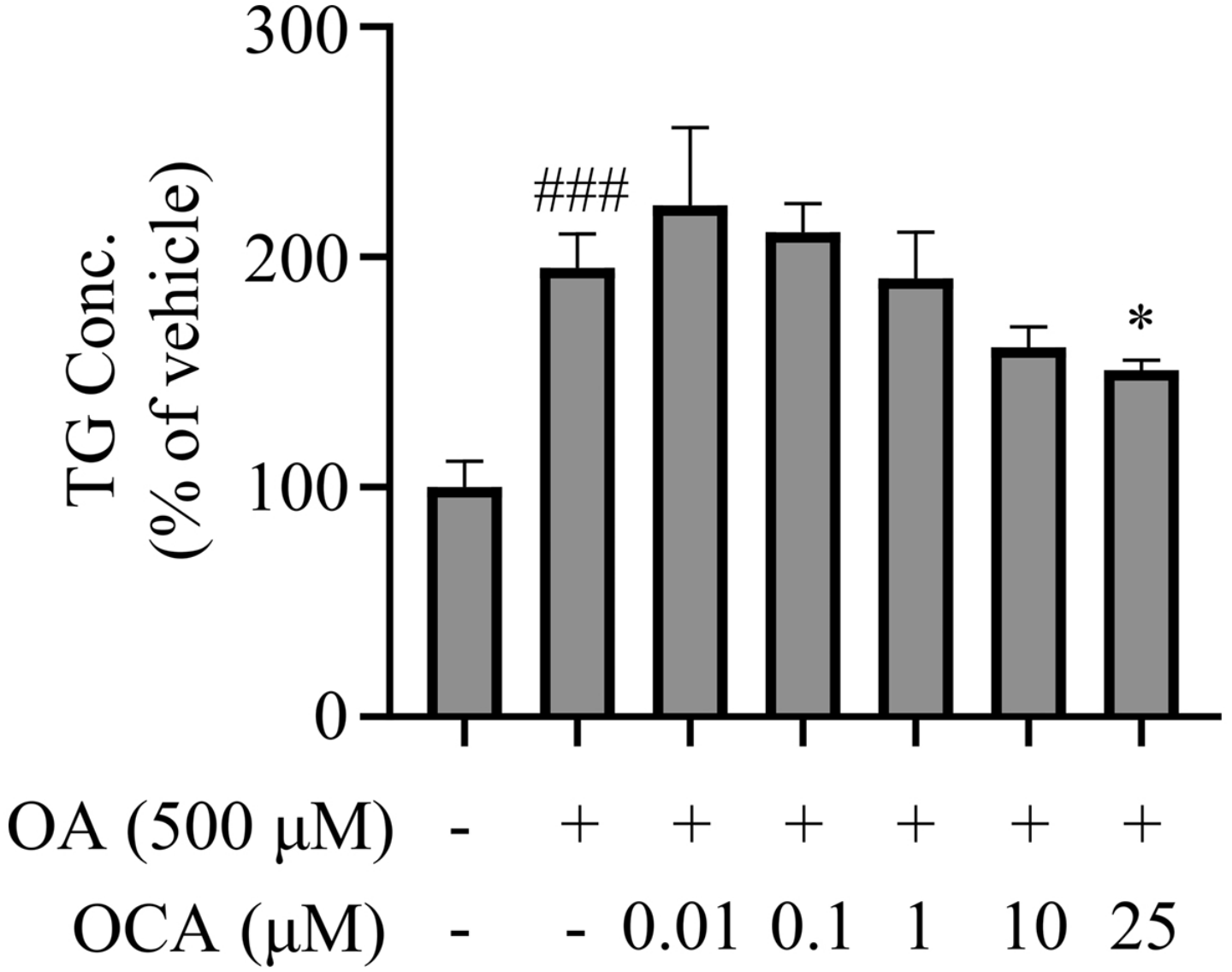

Figure 9

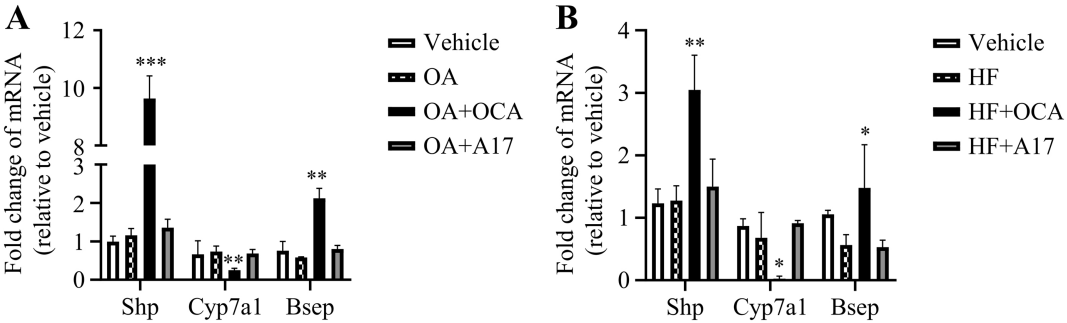
A
Fold change of mRNA (relative to vehicle)
12
10
8
3
2
1
0
***
**
**
Shp
Cyp7a1
Bsep
Vehicle
OA
OA+OCA
OA+A17
B
Fold change of mRNA (relative to vehicle)
4
3
2
1
0
**
*
*
Shp
Cyp7a1
Bsep
Vehicle
HF
HF+OCA
HF+A17

Figure 10

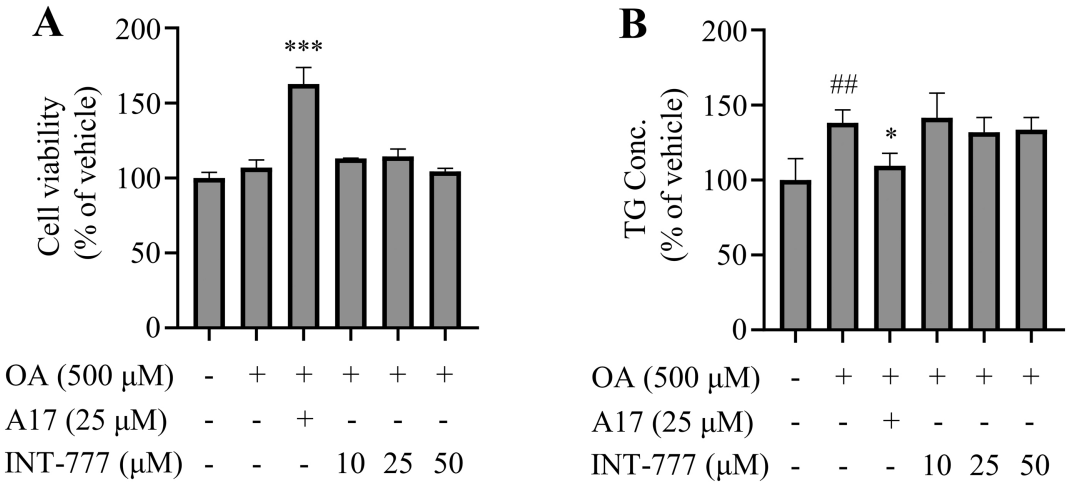
A
Cell viability (% of vehicle)
200
150
100
50
0
***
OA (500 μM) - + + + + +
A17 (25 μM) - - + - - -
INT-777 (μM) - - - 10 25 50
B
TG Conc. (% of vehicle)
200
150
100
50
0
##
*
OA (500 μM) - + + + + +
A17 (25 μM) - - + - - -
INT-777 (μM) - - - 10 25 50

Figure 11

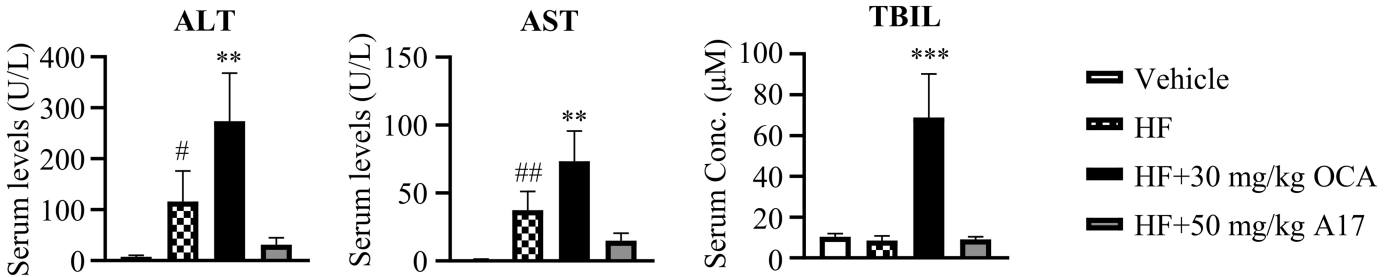
ALT
Serum levels (U/L)
400
300
200
100
0
#
**
AST
Serum levels (U/L)
150
100
50
0
##
**
TBIL
Serum Conc. (μM)
100
80
60
40
20
0
***
Vehicle
HF
HF+30 mg/kg OCA
HF+50 mg/kg A17

Figure 12